3. Results

3.1 Production of HLA-B27 complexes with pLMP2 and pVIPR peptides

3.1.1 HLA-B*2704 and B*2706 production by *in vitro* site-directed mutagenesis

In the Institut für Immungenetik, different subtypes of HLA-B27 were so far investigated, but not B*2704 and B*2706. To prepare complexes of B*2704 and B*2706 with peptides, *in vitro* mutagenesis was used to obtain the mentioned subtypes. As a template for B*2704 production, the B*2705 subtype was used which differs from B*2704 only in three amino acids. This method rests on the PCR reaction which uses the dsDNA of a vector with the inserted gene of HLA-B27 and primers designed to mutate the original DNA sequence. For this experiment B*2705 in the pHN1 vector was used. To prepare the B*2704 subtype, the original B*2705 amino acid sequence was mutated at positions 77 (original D mutated to S), 152 (original V mutated to E) and 211 (original A mutated to G). The final product was sequenced and the sequence was analyzed using Vector NTI Suite 5.5 (Invitrogen) program resulting in a positive clone. This B*2704 clone was taken as template for B*2706 production. Since both residues which differ between B*2704 and B*2706 subtypes are very close to each other, only one primer was used containing two mutations which resulted in amino acid exchanges at positions 114 (H in B*2704 changed to D in B*2706) and 116 (D in B*2704 changed to Y in B*2706). Sequencing and alignment analysis proved that the selected clones had the correct sequence (Figure 3.1).

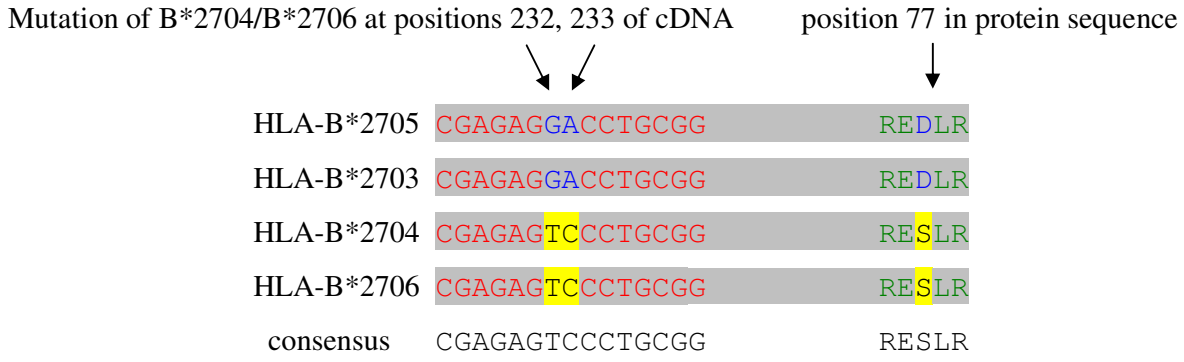

Mutation of B*2704/B*2706 at position 458 of cDNA — position 152 in protein sequence

HLA-B*2705	GCCCGTGTGGCGGAG	ARVAE
HLA-B*2703	GCCCGTGTGGCGGAG	ARVAE
HLA-B*2704	GCCCGTGAGGCGGAG	AREAE
HLA-B*2706	GCCCGTGAGGCGGAG	AREAE
consensus	GCCCGTGTGGCGGAG	ARVAE

Mutation of B*2704/B*2706 at position 635 of cDNA — position 211 in protein sequence

HLA-B*2705	TACCCTGCGGAGATC	YPAEI
HLA-B*2703	TACCCTGCGGAGATC	YPAEI
HLA-B*2704	TACCCTGGGGAGATC	YPGEI
HLA-B*2706	TACCCTGGGGAGATC	YPGEI
consensus	TACCCTGGGGAGATC	YPAEI

Mutation of B*2706 at positions 343 and 349 of cDNA — position 114, 116 in protein sequence

HLA-B*2705	GGGTACCACCAGGACGCCTAC	GYHQDAY
HLA-B*2703	GGTTACCACCAGGACGCCTAC	GYHQDAY
HLA-B*2704	GGTTACCACCAGGACGCCTAC	GYHQDAY
HLA-B*2706	GGGTACGACCAGTACGCCTAC	GYDQYAY
consensus	GGTTACCACCAGGACGCCTAC	GYHQDAY

Figure 3.1. DNA and protein sequence in the mutated regions. The DNA sequence is marked with red color, the protein with green. Introduced mutations are colored in yellow.

3.1.2 Expression of the HLA-B27 subtypes in *E. coli* and purification of inclusion bodies

The pHN1 vector and the construct for expression of β_2m were obtained from Prof. Dr. P. Travers (ICRF, University College, London). The HLA-B*2703 cDNA had formerly been prepared in the Institut für Immungenetik (by Melanie Rühl). B*2704 and B*2706 were made as described above (section 3.1.1). All HLA-B27 complexes are composed of the

extracellular domains of the heavy chain (HC; 32 kDa), β_2-microglobulin (β_2m or light chain; 12 kDa), and a peptide (usually 8-11 amino acids long). The peptides used in the experiments were synthetic and are listed in section Materials and Methods 2.1.6. The extracellular part of HLA-B27 subtypes and β_2-microglobulin were separately expressed in *E. coli* in the form of inclusion bodies. HLA-B*2706 and β_2m were expressed according to the protocol without any changes. B*2703 had to be expressed in a large volume of bacteria culture because of low yield of protein production. For B*2704 the time of growing the culture was extended since it was needed to obtain OD_{560} ~ 0.5. Inclusion bodies were then transferred into soluble form. For this purpose, denaturating conditions (8 M Urea buffer pH 7.5) were used. The unfolded proteins obtained in this way were submitted to the reconstitution buffer in order to create complexes. The concentrations of the inclusion bodies proteins in urea buffer were calculated based on the extinction coefficient of each protein. From 600 ml of bacterial culture we obtained about 9 mg of B*2703, 50 mg of B*2704, 75 mg of B*2706 and 60 mg of β_2m.

To check the quality of produced inclusion bodies, each of the preparations was loaded on SDS gels using reducing conditions (5% SDS, DTT and high temperature). Figure 3.2 illustrates protein inclusion bodies of B*2703, B*2704, B*2706 and β_2m. It shows that the inclusion bodies of these proteins are of good quality, however the B*2704 and B*2706 were not as pure as B*2703 and β_2m.

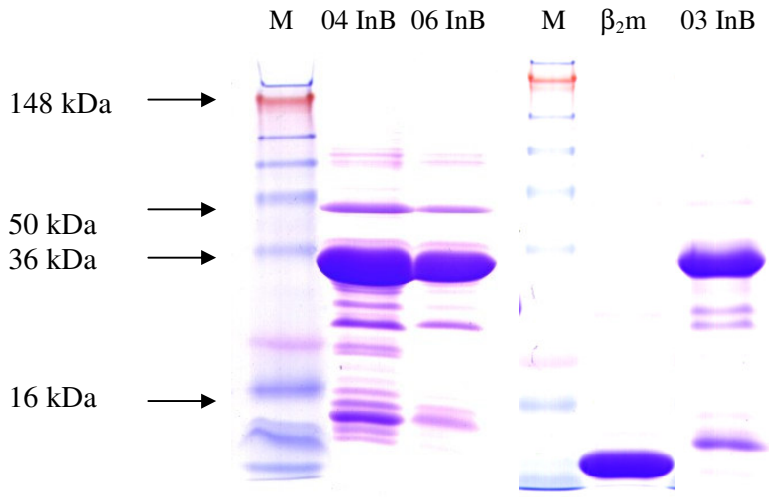

Figure 3.2. Analysis of inclusion body proteins in a 13 % SDS gel. Inclusion body (InB) proteins of B*2703 (03 InB), B*2704 (04 InB), B*2706 (06 InB), and β_2m, 5 µl of each were prepared under reducing conditions. The marker is pre-stained See Blue Plus2.

3.1.3 Reconstitution of HLA-B27:β2m:peptide complexes

The proteins dissolved in urea were set up for refolding with two different peptides which were known to bind to HLA-B27 subtypes. pLMP2 is a viral peptide, composed of 9 amino acids (RRRWRRLTV), and pVIPR (RRKWRRWHL) is a self-peptide. The previously tested time required for complex formation indicated that HLA-B27 subtypes B*2705 and B*2709 need about two weeks for proper refolding. Based on these results, it was assumed that the three subtypes investigated in this study would require a similar time for reconstitution. For complex purification by size exclusion chromatography, the Superdex 75 column was used. It is described in detail below how complexes of each subtype were prepared and purified.

3.1.3.1 Formation of B*2703:β_2m:peptide complexes

HLA-B*2703 is closely related to B*2705, however the expression of it and formation of complexes were definitely less efficient than in case of B*2705 or B*2709. The average amount of inclusion body protein obtained from 600 ml bacteria culture was 9 mg which is very little in comparison to the amount of B*2709 InB, which is about 80 mg/per 600 ml of expression culture. However, the yield of protein was sufficient for refolding of the B*2703 subtype with light chain and peptide. The complexes of B*2703:β_2m:pLMP2 and B*2703:β_2m:pVIPR were each prepared in 400 ml of reconstitution buffer. After two weeks of refolding at 4°C, the complexes were separated from aggregates and free β_2m and foreign peptides by size exclusion chromatography. The results of purification of the sample on Superdex 75 are shown in figure 3.3.

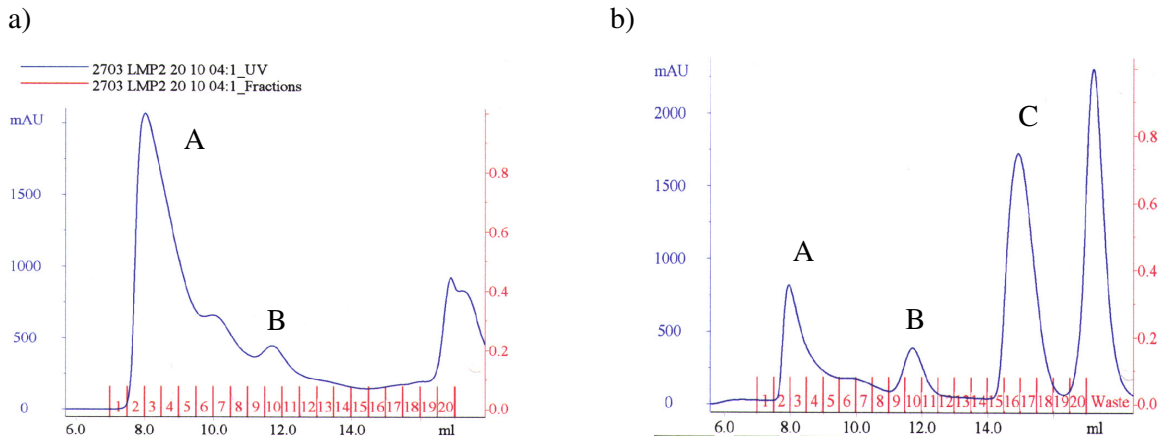

Figure 3.3. Chromatograms of size exclusion purification of B*2703:β_2m:peptides reconstitutions. a) B*2703:β_2m:pLMP2 and b) B*2703:β_2m:pVIPR. Peak A corresponds to aggregates of HLA molecules; peak B represents the complexes whereas peak C corresponds to free β_2m (if it occurs). The peaks around fraction 20 contain waste.

The column was calibrated with BSA (67 kDa), Ovalbumin (43 kDa), Chymotrypsin A (25 kDa), Cytochrome C (12.5 kDa) and Aprotinin (6.5 kDa). This allowed to estimate that the desired complexes should be present in fraction 10. This fraction in case of B*2703:β_2m:pVIPR (Figure 3.3) contains a definite peak (B) which may indicate that the protein is of greater purity than the B*2703:β_2m:pLMP2 complex, also obtained in fraction 10, where the peak (B) is not that well defined.

The fractions corresponding to peaks in the chromatograms were analyzed with SDS gels in order to verify whether fraction 10 contains B*2703:β_2m:pLMP2 or B*2703:β_2m:pVIPR complex. The gels obtained under reducing conditions are shown in figure 3.4.

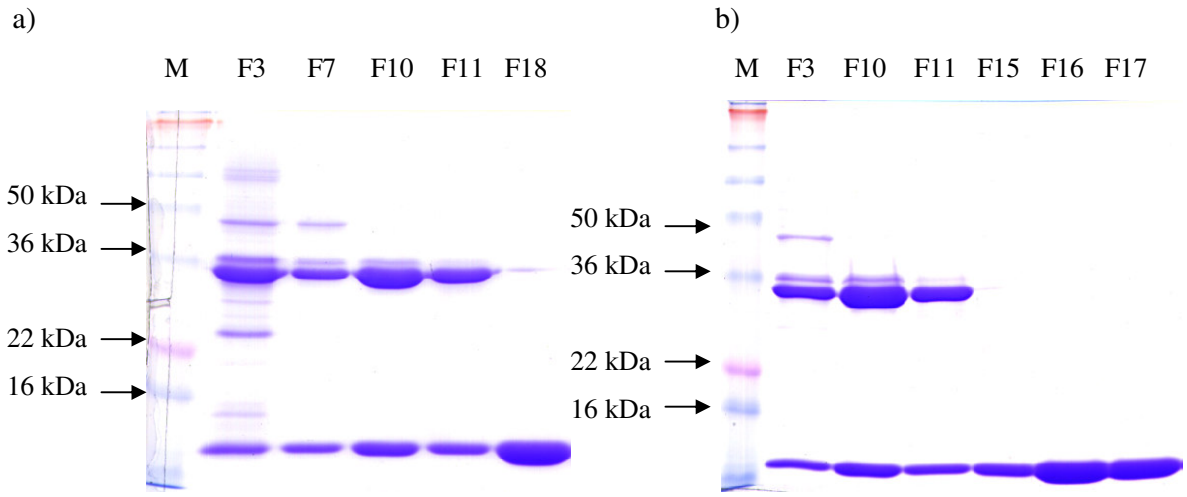

Figure 3.4. Analysis of FPLC fractions of size exclusion on 13 % SDS. a) B*2703:β_2m:pLMP2 complex, b) B*2703:β_2m:pVIPR complex. Both gels were done under reducing conditions. The molecular weigh marker (M) is See Blue Plus2. F3, F7, F10, F11, F15, F16, F17 and F18 correspond to fraction numbers in FPLC runs. From each fraction 20 µl were loaded on the gels. As supposed from the size, fractions 10 contain pure complexes of B*2703 with peptides.

Both gels show that the complexes were of good purity. The upper band refers to the heavy chain (32 kDa) and the lower one to the light chain β_2m (about 12 kDa). The stoichiometric ratio of heavy to light chain is in the same range in both complexes. Fractions (9, 10, 11) containing complex (B*2703:β_2m:pLMP2 or B*2703:β_2m:pVIPR) were combined, and the concentration was calculated. For each complex about 0.4 mg/ml was obtained. Complexes of proteins with the highest purity were concentrated to 12 mg/ml, and 25 µl of the protein complex were used for crystallization.

3.1.3.2 Formation of B*2704:β_2m:peptide complexes

Similar to B*2703, the B*2704 subtype also proved difficult to express. The bacterial cells containing plasmid with the B*2704 subtype grew very slowly and needed about twice as much time as the other subtypes to obtain OD ~ 0.5. In this case two different deviations from the protocol were tried, and both worked well. Either the culture was grown during the day and put to the fridge overnight to induce it next day at 37°C, or the culture was grown overnight at lower (room) temperature and induced next morning at 37°C. In both cases we were able to obtain inclusion bodies at concentrations about 50 mg/600 ml bacteria culture. This amount was sufficient to test different conditions of complex formation. The standard refolding set-up of

B*2704:β_2m:pLMP2 provided about 0.2 mg/ml of pure complex and a large amount of aggregates. The amount of this subtype with pVIPR peptide was even lower.

a) b)

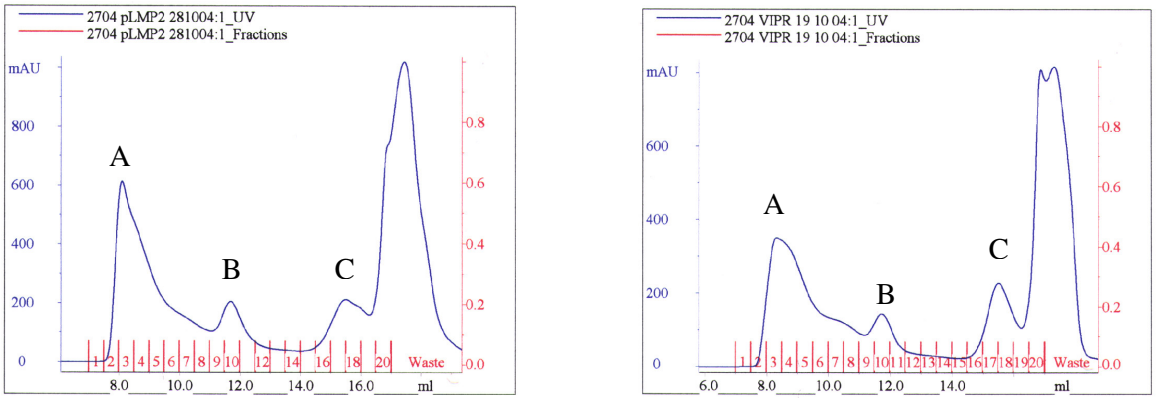

Figure 3.5. Chromatograms representing size exclusion purification results of B*2704 complexes with pLMP2 and pVIPR. a) HLA-B*2704:β_2m:pLMP2 and b) HLA-B*2704:β_2m:pVIPR. Peak A corresponds to aggregate, peak B corresponds to ternary complexes, and peak C contains free β_2m.

Large amounts of aggregates are seen in fractions 2-4, in comparison with small amount of pure protein complexes obtained in fraction 10. Despite of that the crystallization set-ups were performed using conditions which were already tested for B*2705 and B*2709.

To improve the yield of complexes of B*2704:β_2m:pLMP2 and B*2704:β_2m:pVIPR, the following conditions for reconstitution set-ups were tried: double amount of HC with standard amounts of light chain and peptide as well as fourfold amount of HC with double amounts of β_2m and peptide. No significant improvements were seen in any of these trials.

All above mentioned conditions were repeated using freshly prepared inclusion bodies of all components and fresh peptides; however, it still was not able to produce complexes in suitable amounts for crystallization. Finally 20 % of glycerol was added to the reconstitution buffer, to check whether this would stabilize the complexes. After two weeks of refolding at 4°C the complexes were purified by size exclusion chromatography using a Superdex 75 column. Complexes of B*2704:β_2m:pLMP2 and B*2704:β_2m:pVIPR were obtained at amounts of 1.3 mg/ml. The amount of the aggregates was this time lower than that of the complexes (Figure 3.6).

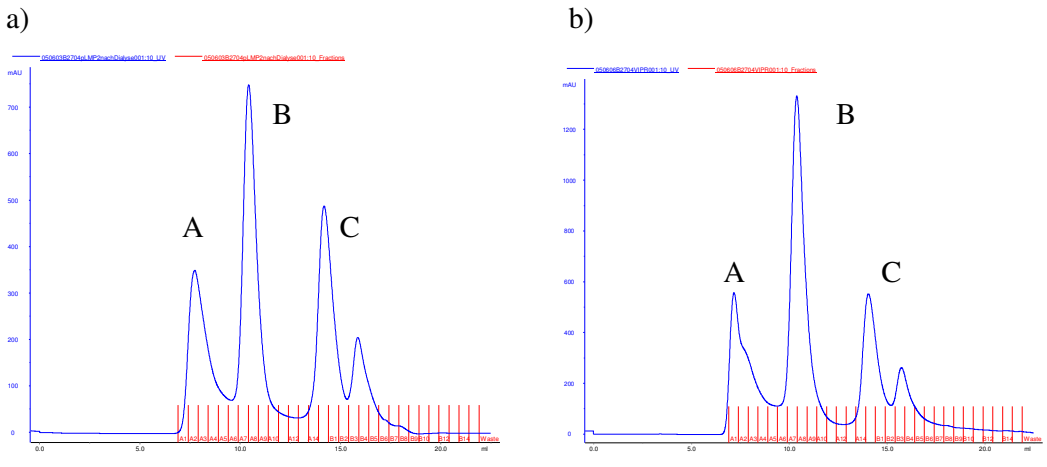

Figure 3.6. Chromatograms of size exclusion purification of B*2704:β_2m:peptides reconstitutions. a) B*2704:β_2m:pLMP2 and b) B*2704:β_2m:pVIPR. Peak A – aggregate, peak B – ternary complex of B*2703:β_2m:peptide, peak C – free β_2m.

The peaks (B) which correspond to HLA-B2704:β_2m:peptide complexes were sharp and narrow, indicating that they were of good purity. The complexes were obtained this time from different fractions since the other Superdex 75 column was used, however, the difference in the elution position of the complex correlates with the position of the calibration proteins. The column calibration showed that fractions 7-9 should contain the ternary complexes (about 44 kDa).

These and other fractions which corresponded to peaks in the chromatograms were loaded on the SDS gel in order to check the purity of the obtained complexes (Figure 3.7).

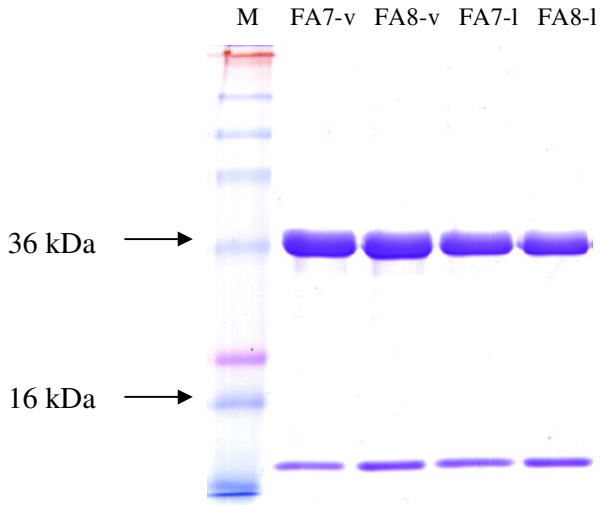

Figure 3.7. Analysis of FPLC fractions of B*2704:β_2m:peptides purification on a 13 % SDS gel. SDS gel represents fractions of FPLC run (Fig 3.6 a and b) under reducing conditions. 20 µl of each fraction were loaded on the gel with pre-stained marker See-Blue Plus2. FA7-v and FA8-v contain components of the complex of B*2704 with pVIPR whereas FA7-l and FA8-l refer to the complex of the same subtype with pLMP2 peptide.

Both gels indicate that the obtained proteins are of good quality and contain all components (HLA-B*2704, β_2m and peptide). The higher band at about 32 kDa corresponds to HLA-B27 heavy chain, whereas the band at 12 kDa contains β_2m. Since for crystallization of proteins the highest purity is very important, only fraction 8 containing the top of the peak (about 1.3 mg/ml) was concentrated to 12 mg/ml, and 100 µl of pure complex was taken for crystallization set-ups.

3.1.3.3 Formation of B*2706:β_2m:peptide complexes

From three subtypes which were investigated in this study B*2706 was the one which was less problematic both in expression and complex formation. This is surprising since B*2704 and B*2706 differ only in two amino acids.

Sufficient amounts of B*2706 inclusion bodies were produced to test different conditions in which this subtype forms complexes with β_2m and peptide. In 600 ml bacterial culture approximately 75-80 mg of inclusion body protein was obtained. The reconstitution of B*2706:β_2m:pLMP2 and B*2706:β_2m:pVIPR followed standard procedures and provided large amounts of B*2706:β_2m:pLMP2 complex (about 0.76 mg/ml) while the amount of B*2706:β_2m:pVIPR complex was two times less. Differences in the FPLC chromatograms of both peptide complexes were also noticed, B*2706:β_2m:pLMP2 did not form much aggregates whereas the reconstitution with pVIPR always resulted in large amounts of aggregate and smaller yield of complex. This could mean that peptide pVIPR causes aggregation, which was not observed before (Figure 3.8).

a) b)

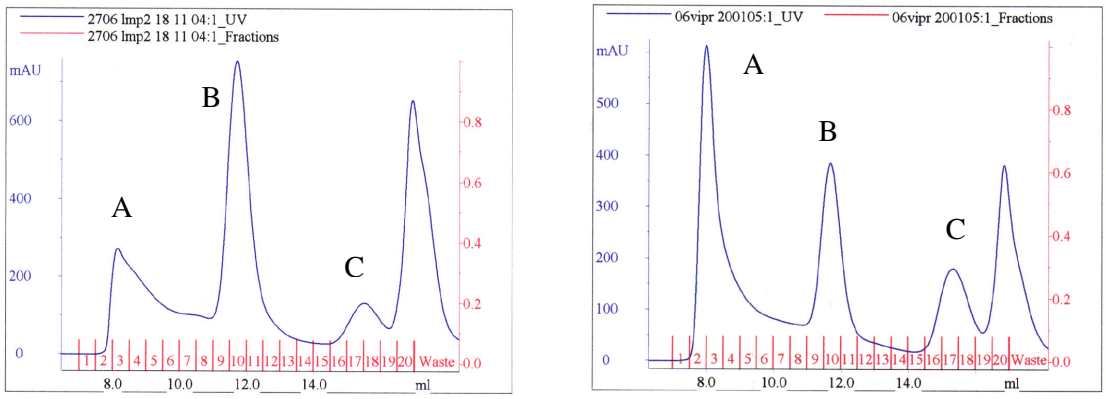

Figure 3.8. Chromatograms representing size exclusion purification results of B*2706 complexes with a) pLMP2 and b) pVIPR. Calibration of the column allows to estimate that on both chromatograms the A peak corresponds to aggregate, B peak contains B*2706:β_2m:peptide complexes and C peak corresponds to free β_2m.

In the complex with the peptide pLMP2, most of the protein was present in the ternary form and was obtained in fractions 9-11. Purification of B*2706:β_2m:pVIPR gave also reasonable amounts of complex but the yield of aggregates was much larger.

To minimize the aggregation of B*2706:β_2m:pVIPR, additional conditions of refolding were tested. Neither the double amount of HC with one part of β_2m and peptide nor four parts of HC with double amount of β_2m and pVIPR prevented aggregate formation. However, in the presence of the double amount of HC with standard β_2m and pVIPR amounts, more protein was formed in the correct heterotrimeric form (B*2706:β_2m:pVIPR) than in aggregates (Figure 3.9). The chromatogram showed that fractions 9, 10 and 11 should correspond to the complex. To verify whether the complex contains all components, selected fractions were run on an SDS gel. Results are shown in figure 3.10.

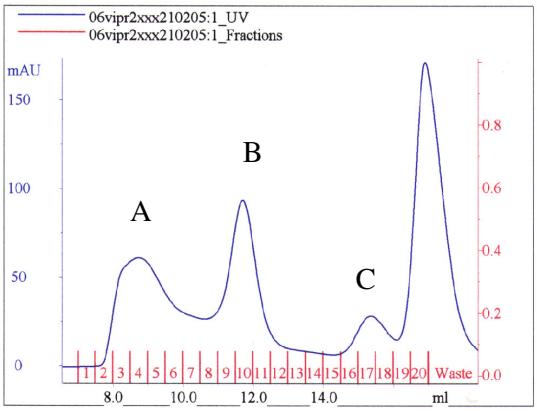

Figure 3.9. Chromatogram representing size exclusion purification of B*2706 in complex with pVIPR peptide. Peak B corresponds in size to the heterotrimer. The amount of aggregate (peak A) is lower than the amount of complex. Peak C represents β_2m.

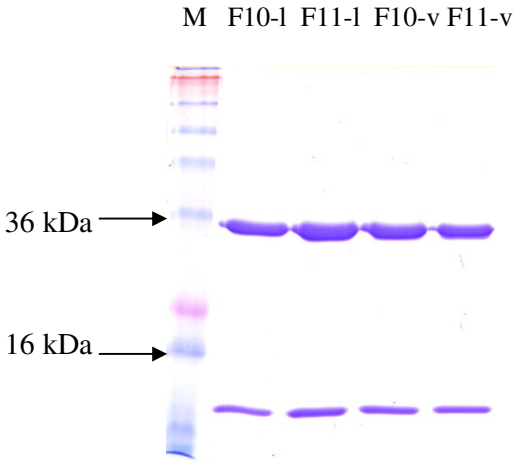

Figure 3.10. SDS gel representing fractions of the FPLC run (Figure 3.9) containing B*2706:β_2m:peptide complexes. The 13 % SDS gel was run under reducing conditions in order to separate components of complexes. F10-l and F11-l correspond to B*2706:β_2m:pLMP2, F10-v and F11-v to B*2706:β_2m:pVIPR. The molecular weight marker (M) is pre-stained See-Blue Plus2.

The gel run under reducing conditions proves that fractions 10 and 11 contain HC and β_2m. The upper band is about 32 kDa, and this is the size of extracellular domain of HLA-B*2706, the lower band corresponds to β_2m (about 12 kDa). The purified protein was concentrated to 12 mg/ml, and the yield of 30 µl was used for crystallization.

3.2 Crystallization of purified HLA-B27 complexes

For crystallization set-ups those fractions of purified heterotrimeric complexes were taken which corresponded to the whole peak containing the complex (F9, F10, F11 of B*2703 complexes) or to the maximum peak (FA8 of B*2704 complexes and F10 of B*2706 complexes). For crystallization the protein was normally concentrated to 12 mg/ml, however sometimes the protein was less concentrated due to severe precipitation during crystallization.

All crystallization trials with HLA-B27:β_2m:peptide complexes were performed in hanging-drop vapor diffusion setups at 18°C by mixing 1.5 µl protein solution and 1.5 µl precipitant solution. We employed conditions which have previously been described for B*2705 and B*2709 in complexes with various peptides (Hülsmeyer et al., 2002; Hülsmeyer et al., 2005; Hillig et al., 2004). Crystal formation for all three complexes was optimized by varying the polyethylene glycol (PEG) concentration in the precipitant solution, 18-28% (w/v) PEG 8000, 100 mM Tris/HCl, pH 7.0 for B*2703 complexes, 18-28% (w/v) PEG 8000 or PEG 6000, 100 mM Tris/HCl, pH 7.0 for B*2704 complexes, and 18-28% (w/v) PEG 8000, PEG 6000 or PEG 4000, 100 mM Tris/HCl, pH 7.0 for B*2706 complexes. To initiate crystallization or when the initially obtained crystals were too small for X-ray diffraction experiments, streak seeding was applied by passing a whisker hair of a cat through each crystallization drop.

Prior to data collection, the crystals had to be fished from the crystallization drops using a nylon loop and cryo-protected by stepwise increasing glycerol to final concentrations of 10%. The crystals were subsequently frozen in liquid nitrogen.

X-ray data collection as well as phasing and structure determination was performed by the cooperating group of Prof. W. Saenger in the Institut für Chemie und Biochemie/Kristallographie at the Freie Universität Berlin.

3.2.1 Crystallization of B*2703:β_2m:peptide complexes

The crystals of B*2703:β_2m:pVIPR grew after 4 days as plates to a maximum size of 200 x100 x10 µm at 18% (w/v) PEG 8000. The crystals of B*2703:β_2m:pLMP2 (Figure 3.11) had identical morphology, but were always smaller than those from B*2703:β_2m:pVIPR with approximate dimensions of 80 x 80 x 5 µm obtained at 22% (w/v) PEG 8000 (Loll at al., 2005 a).

a) b)

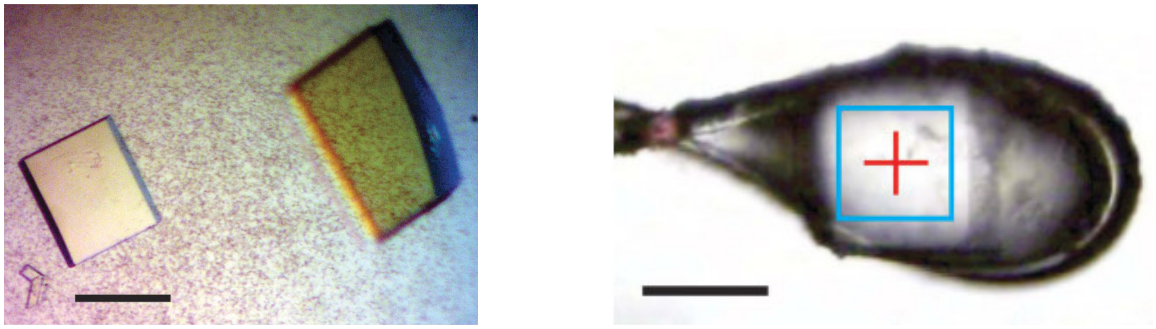

Figure 3.11. Crystals of B*2703:β_2m:pLMP2. The black bar indicates a length of 80 µm. Crystals of B*2703:β_2m:pVIPR exhibited the same morphology but were slightly larger (not shown). a) Crystals within the crystallization drop, b) Cooled crystal mounted in a cryoloop at beamline ID14-2 (ESRF) equipped with a mini-diffractometer. The rectangle in cyan represents the size of the X-ray beam.

3.2.2 Crystallization of B*2704:β_2m:peptide complexes

After 4 days, B*2704:β_2m:pVIPR crystallized from a precipitant solution composed of 28% (w/v) PEG 8000, 100 mM Tris/HCl pH 7.0, and crystals of B*2704:β_2m:pLMP2 were obtained from a solution mixed of 26% (w/v) PEG 6000, 100 mM Tris/HCl pH 7.0 (Loll et al., 2005 b). The crystals of both subtypes grew to a maximum size of about 80 x 20 x 10 µm and had similar size and morphology. Crystals of B*2704:β_2m:pLMP2 are shown in figure 3.12.

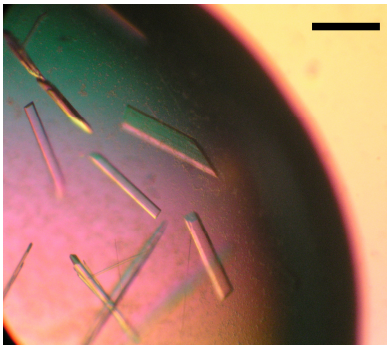

Figure 3.12. Crystals of B*2704:β_2m:pLMP2. The black bar indicates a length of 50 µm. Crystals of B*2704:β_2m:pVIPR exhibited comparable size and morphology (not shown).

3.2.3 Crystallization of B*2706:β_2m:peptide complexes

After 4 days, crystals of B*2706:β_2m:pLMP2 were obtained from a solution containing 24% (w/v) PEG 8000, 100 mM Tris/HCl pH 7.0, and B*2706:β_2m:pVIPR crystallized using a precipitant solution composed of 20% (w/v) PEG 8000, 100 mM Tris/HCl pH 7.0 (Zawacka et al., 2005). The crystals of both subtypes grew to a maximum size of about

80 x 20 x 10 µm in one week and had similar size and morphology. Crystals of B*2706:β_2m:pVIPR are shown in figure 3.13.

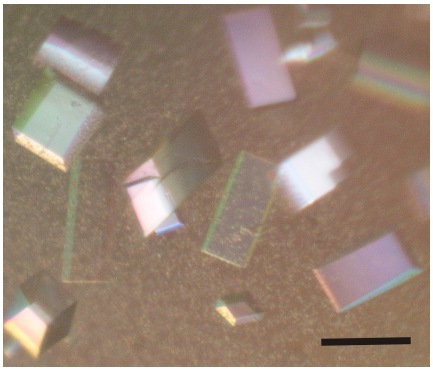

Figure 3.13. Crystals of B*2706:β_2m:pVIPR. The black bar indicates a length of 80 µm. Crystals of B*2706:β_2m:pLMP2 exhibited comparable size and morphology (not shown).

3.3 Structural and thermodynamic features of HLA-B27 complexes

All crystal structures were determined using molecular replacement. As search model, the structures of two B*2705 complexes were used since this subtype differs from the investigated ones only in a few polymorphic amino acids. For determining the structures of B*2703 and B*2704 complexes, the structure of B*2705:β_2m:pVIPR (Hülsmeyer et al., 2004), with the protein data bank (PDB) accession code 1OGT was used. In solving the structure of B*2706 complexes, B*2705:β_2m:pGR (Rückert et al., 2005) with the PDB code 2A83 was used. For molecular replacement all water molecules, the peptide as well as polymorphic residues were omitted.

3.3.1 Overview of HLA-B27 structures in complexes with pLMP2 and pVIPR

3.3.1.1 Features of B*2703 in complex with pLMP2 and pVIPR

The crystals of B*2703 subtype diffracted to 2.0 Å (B*2703:β_2m:pLMP2) and 1.55 Å (B*2703:β_2m:pVIPR) resolution but were not isomorphous (Table 3.1), which contrasts the B*2705 and B*2709 subtypes (space group $P2_1$, each in complex with pLMP2 and pVIPR), (Fiorillo et al., 2005). However for B*2705 and B*2709 subtypes in complex with m9 (Hülsmeyer et al., 2002) and TIS (Hülsmeyer et al., 2005) peptides, space group $P2_12_12_1$ was reported.

Table 3.1 Data collection and refinement statistics of B*2703:β_2m:pLMP2 and B*2703:β_2m:pVIPR

Subtype		**B*2703:β_2m:pLMP2**	**B*2703:β_2m:pVIPR**
Data collection			
Space group		$P2_12_12_1$	$P2_1$
Unit cell a; b; c [Å]		50.7; 82.6; 108,3	50.9; 81.6; 65.3
α; β; γ [°]		90; 90; 90	90; 107; 90
Resolution [Å] [a]		20.0 – 2.0 (2.03 – 2.00)	30.0 - 1.55 (1.58 – 1.55)
Unique reflections		30890 (1512)	70574 (3112)
Completeness		98.3 (97.3)	95.3 (85.1)
Redundancy		4.2 (3.7)	3.1 (2.7)
$\langle I/\sigma(I)\rangle$		16.3 (3.9)	22.2 (3.4)
R_{sym} [a]		0.074 (0.301)	0.045 (0.281)
Refinement			
Non-hydrogen atoms		4331	4141
R_{cryst} [a, b]		0.134 (0.155)	0.127 (15.0)
R_{free} [a, c]		0.177 (0.179)	0.150 (0.170)
Heavy chain,	no. of atoms / average B factor [Å^2]	2372 / 11.9	2383 / 14.8
β_2m,	no. of atoms / average B factor [Å^2]	893 / 13.8	867 / 16.6
Peptide,	no. of atoms / average B factor [Å^2]	129 / 11.9	168 / 13.9
Water,	no. of molecules / average B factor [Å^2]	868 / 31.4	710 / 30.9
Glycerol,	no. of atoms / average B factor [Å^2]	36 / 28.3	36 / 36.0
Rmsd [d] from ideal geometry,	bond length [Å]	0.012	0.012
	bond angles [°]	1.59	1.48

[a] values in parentheses refer to the highest resolution shell
[b] $R_{cryst} = \Sigma_h \left| F_o - F_c \right| / \Sigma F_o$ (working set, no σ cut-off applied)
[c] R_{free} is the same as R_{cryst}, but calculated on 5 % of the data excluded from refinement.
[d] Root-mean-square deviation (Rmsd) from target geometries.
An initial data set for B*2703:pVIPR was collected at the Protein Structure Factory beamline BL14.2 of the Freie Universität Berlin at BESSY, Berlin, Germany. Datasets with the highest diffraction limit were collected at the European Synchrotron Radiation Facility (ESRF, Grenoble, France), beamline ID 14-2, at a wavelength of λ = 0.933 Å at 100 K.

Both protein complexes show the characteristic fold of MHC class I molecules (Madden, 1995). The electron density maps are well defined allowing for unambiguous modeling of proteins and peptides in the binding grooves of B*2703 (Figure 3.14). Apart from the peptides, the B*2703 complexes are nearly identical (Cα root mean square deviation of 0.568 Å). Differences are restricted to solvent-exposed amino acid side chains and the peptide conformation.

a) b)

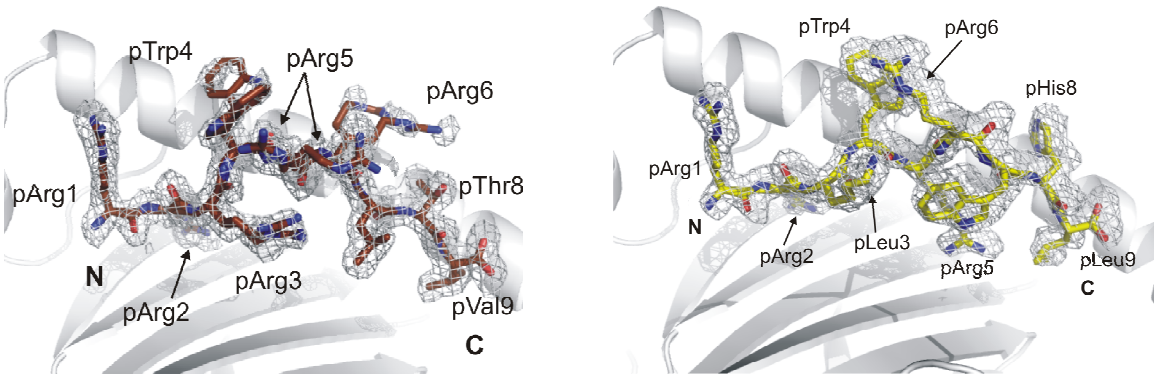

Figure 3.14. The topography and electron densities of peptides bound to the B*2703 subtype. The conformation of the peptides a) pLMP2 and b) pVIPR in B*2703 viewed from the α2-helix together within ribbon representation of the α1-helix and the floor of the binding groove. α2-helix has been removed for better visualization. In case of pLMP2, pArg5 points towards the viewer, in pVIPR, pArg5 is directed to the bottom of the binding groove. Final $2F_o$-F_c electron densities are contoured at the 1 σ level.

A metal binding site with an octahedral coordination sphere was identified only in B*2703:β_2m:pVIPR. The metal cation is coordinated by pHis8-NE of the peptide and His197-NE of the heavy chain of a neighbouring molecule as well as by four water molecules. The metal was interpreted as Mn^{2+} due to its coordination distances (Harding, 2001) and the fact that a similar binding site was identified in the structure of B*2705:β_2m:pVIPR and B*2709:β_2m:pVIPR (Hülsmeyer et al., 2004). Most likely the Mn^{2+} originates from the lysis buffer.

The N-termini of both peptides (pArg1 and pArg2) occupy identical positions (Figure 3.15 and Table 3.2). The side chain of pArg1 is sandwiched between Arg62 located on the α1-helix and Trp167 on the α2-helix. At the C-termini (the F pockets), there are no significant differences between both subtypes. The C-terminus of the bound pLMP2 peptide is buried in the B*2703 subtype slightly deeper than that of pVIPR (difference of 1.86 Å at p7 between peptides), possibly as a consequence of altered p3–p7 conformations. The hydrophobic pLeu9 of B*2703:β_2m:pVIPR and the pVal9 of B*2703:β_2m:pLMP2 are pointing into the F-pocket. The C-termini receive the common stabilization by Tyr84OH, Thr143OG1 and Lys146NZ1 (Table 3.2), and the aliphatic amino acid side chains of the two p9 residues are further stabilized by hydrophobic interactions with residues of the HC.

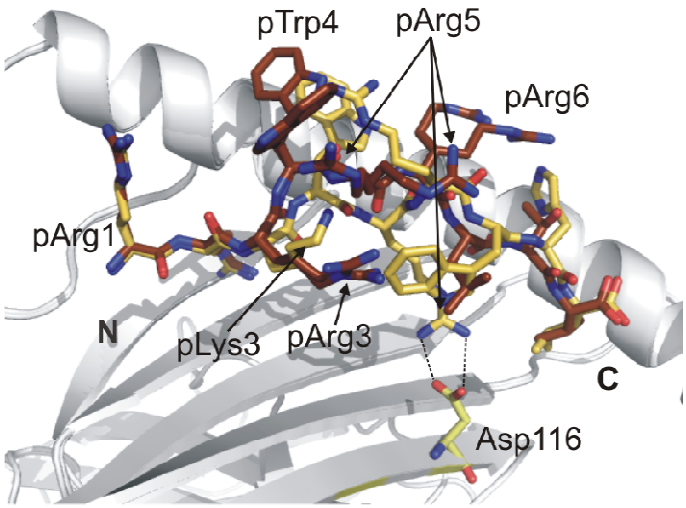

Figure 3.15. pLMP2 and pVIPR topographies when bound to subtype B*2703. Overlay of B*2703:β_2m:pLMP2 (brown) and B*2703:β_2m:pVIPR (yellow) structures. The salt bridge between pArg5 and Asp116 in B*2703:β_2m:pVIPR is marked with dashed lines. The α2-helix was removed for better visualization of the peptides.

Unexpectedly, the peptides are bound to the binding groove of B*2703 in drastically different fashions. The major structural difference is found for pArg5 and for the overall conformation of the middle section of the peptide (Figure 3.15 and Table 3.2). This part (residues p3 to p7) is usually accessible for recognition by a TCR. In the B*2703:β_2m:pVIPR structure, the peptide is bound in the non-canonical conformation p6α (main chain φ/ψ torsion angles in α-helical conformation at p6, φ/ψ) with the side chain of pArg5 pointing towards the binding groove. The guanidinium group of pArg5 forms a bidentate salt bridge (3.05 Å) to Asp116 which is located on the floor of the binding groove (Table 3.2). pTrp4 and pArg6 are solvent exposed and stabilized by π-stacking of the indole ring of Trp and the guanidinium group of Arg.

Table 3.2 Comparison of pLMP2 and pVIPR coordinations in the HLA-B*2703 subtype. Only direct intrapeptide contacts and contacts between peptides and HC residues are included, and solvent-mediated interactions are omitted for the sake of clarity. van der Waals' contacts are not given explicitly for each amino acid. Water mediated contacts between protein and the peptides are not listed for sake of clarity. In the B*2703:β_2m:pLMP2 structure, pArg3, pTrp4, pArg5, pArg6 and Glu76 occur in alternative conformations. Only one of the equally occupied conformations is shown in the table.

Peptide position	B*2703:β_2m:pLMP2				B*2703:β_2m:pVIPR			
	Peptide residue	**Contact residue**	**Distance [Å]**	**Interaction**	**Peptide residue**	**Contact residue**	**Distance [Å]**	**Interaction**
p1	pArg1^{N}	Tyr7^{OH}	3.2	HB	pArg1^{N}	Tyr7^{OH}	3.2	HB
	pArg1^{N}	Tyr171^{OH}	2.7	HB	pArg1^{N}	Tyr171^{OH}	2.7	HB
	pArg1^{NE2}	Glu163^{OE1}	3.0	SB	pArg1^{NE2}	Glu163^{OE1}	3.2	SB
	pArg1^{NH2}	Glu163^{OE1}	3.5	SB	pArg1^{NH2}	Glu163^{OE1}	3.5	SB
	pArg1^{NH2}	Glu163^{OE2}	3.1	SB	pArg1^{NH2}	Glu163^{OE2}	3.0	SB
	pArg1^{NH1}	Arg62^{NE}	3.6	HB	pArg1^{NH1}	Arg62^{NE}	3.5	HB
	pArg1^{O}	Tyr159^{OH}	2.7	HB	pArg1^{O}	Tyr159^{OH}	2.7	HB
p2	Contacts formed by Arg2 are very similar in both complexes							
p3	pArg3^{N}	Tyr99^{OH}	2.9	HB	pLys3^{N}	Tyr99^{OH}	2.9	HB
	pArg3	Tyr99, Leu156, Tyr159	3.6-4.0	vdW	pLys3^{NZ}	pTrp4^{O}	2.9	HB
					pLys3	Tyr99, Tyr159		vdW
	pArg3^{NH2}(A)	pArg5^{ND1} (A)	2.9	HB				
	pArg3^{NH1}	Gln155^{O}	3.1	HB				
	pArg3^{NH2}	pArg^{O}	3.2	HB				
p4	The side chain of this residue is solvent-exposed in both complexes							
	pTrp4O	pArg6^{N}	3.4	HB	pTrp4^{O}	pLys3^{NZ}	2.9	HB
	pTrp4	Arg62 Gln65, Ile66	3.6-4.0	vdW	pTrp4	Ile66, Ala69	~3.3	vdW
p5	pArg5^{ND1}(A)	pArg3^{NH2}(A)	2.9	HB	pArg5^{NH1}	Asp116^{OD1}	3.0	SB
	pArg5^{NE2}	Gln155^{OE1}	2.8	HB	pArg5^{NH1}	Asn97^{OD2}	3.1	HB
p6	The side chain of this residue is solvent-exposed in both complexes							
	pArg6^{NH1} (B)	Glu76^{OE1} (A)	3.0	SB	pArg6^{NH1}	pTrp4^{O}	3.3	HB
					pArg6	pTrp4	~3.3	vdW
p7	pLeu7	His114, Trp147	~3.5	vdW	pTrp7	Leu156	~3.5	vdW
p8	The side chain of this residue is solvent-exposed in both complexes							
	pThr8^{OG1}	Lys146^{NZ}	2.8	HB	pHis8^{ND1}	Asp77^{OD1}	2.8	HB
	pThr8^{O}	Lys146^{NZ}	2.9	HB	pHis8^{O}	Trp147^{NE1}	2.8	HB
	pThr8^{O}	Trp147^{NE1}	2.9	HB	pHis8^{O}	Leu9^{OXT}	3.3	HB
	pThr8	Glu76, Asp77		vdW				
p9	pVal9^{N}	Asp77^{OD1}	3.0	HB	pLeu9^{N}	Asp77^{OD1}	3.0	HB
	pVal9^{O}	Thr146^{OG1}	3.2	HB	pLeu9^{O}	Thr143^{OG1}	2.7	HB
	pVal9^{O}	Tyr84^{OH}	3.0	HB	pLeu9^{O}	Tyr84^{OH}	2.7	HB
	pVal9^{OXT}	Tyr84^{OH}	3.0	HB	pLeu9^{OXT}	Tyr84^{OH}	3.4	HB
	pVal9^{OXT} (B)	Thr143^{OG1}	2.7	HB	pLeu9^{OXT}	Thr146^{NZ}	~3.0	HB

In contrast, pLMP2 adopts the classical conformation termed p4α (main chain φ/ψ torsion angles in α-helical conformation at p4), with the side chain of Arg5 protruding out of the peptide binding groove and being exposed to solvent. The side chains of pTrp4 and pArg6 bulge out of the peptide binding groove as well (Figure 3.15). As a consequence, the solvent exposed area

differs in both structures and could result in different recognition by a TCR. Comparing the number of double conformations within both bound peptides, pLMP2 peptide complexed with B*2703 reveals double conformations for the solvent exposed amino acids (p3 to p6) (Figure 3.15) whereas for B*2703:β_2m:pVIPR, no double conformation is observed. This might indicate a higher degree of flexibility of pLMP2 complexed by B*2703, as further evidenced by higher B-factors within the peptide residues of pLMP2 (Figure 3.16). The higher resolution of HLA-B*2703:β_2m:pVIPR complex (1.55 Å) indicates also that this structure is better defined and more stable than in case of HLA-B*2703:β_2m:pLMP2 (2.0 Å).

a) b)

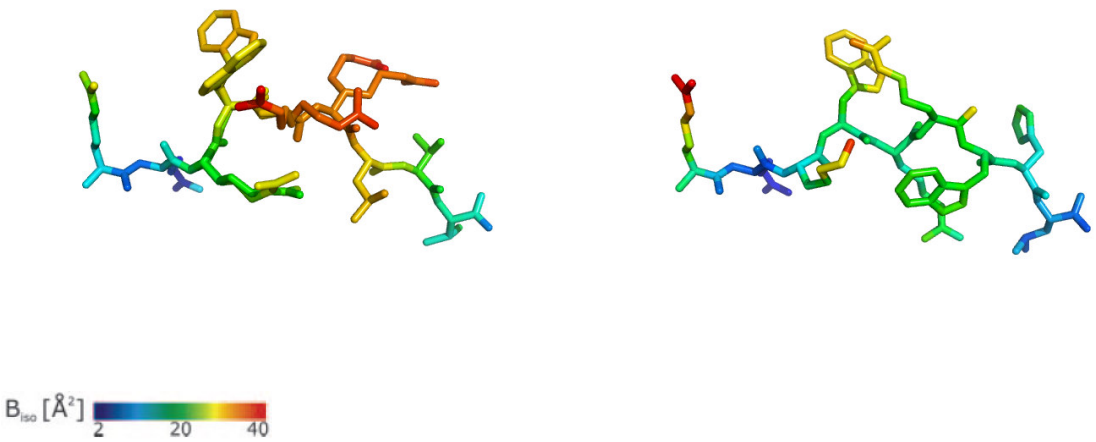

Figure 3.16. B factor representation for pLMP2 and pVIPR complexed with B*2703. a) pLMP2 color-coded by isotropic B factor, b) pVIPR color-coded by isotropic B factor.

The replacements of Tyr59 in B*2703 (by His59) and in B*2717 (by Phe59) are the only ones that are known to affect this residue for more than 1000 alleles of the six HLA class I loci. Solving the two crystal structures of the B*2703 subtype allowed to investigate whether any structural differences exist in the A-pocket as a result of the Tyr to His exchange at position 59 of the HC. Tyr at position 59 was shown to participate in forming hydrogen bonds in the A-pocket, and its substitution by His59 could have a destabilizing effect on the N-terminus of the peptide.

The classical hydrogen bonding network (Madden et al., 1992; Madden, 1995) in the A-pocket of HLA-B27 molecules is formed by three highly conserved tyrosine residues (Tyr59, Tyr7 and Tyr171), Glu45 of the HC and a water molecule (Figure 3.17). Whereas Tyr59, Tyr7 and Tyr171 are in hydrogen bonding distance to the N-terminus of the peptide, Glu45 of the HC is indirectly linked via a single water molecule.

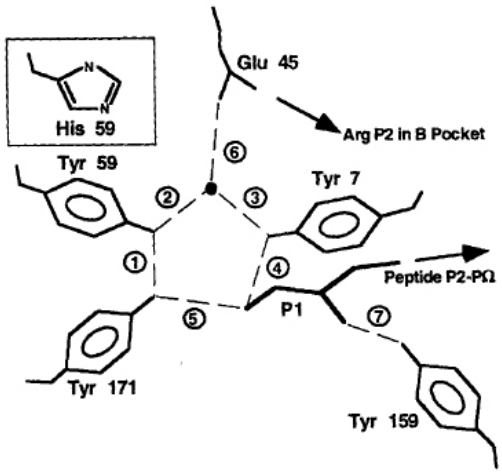

Figure 3.17. The classical hydrogen bonding network within the A-pocket (Griffin et al., 1997). Schematic diagram of A pocket hydrogen bonds. Conserved tyrosines at positions 7, 59 and 171 form a pentagonal H bond network with a water molecule (black dot) and the N-terminus (P1) of a peptide. The His59 side chain which replaces Tyr59 in B*2703 is shown in the inset.

The crystal structures of B*2703 reveal that the overall architecture of the A-pocket remains unchanged compared with the known structures of HLA-B27:β_2m:peptide complexes (Figure 3.18).

a) b)

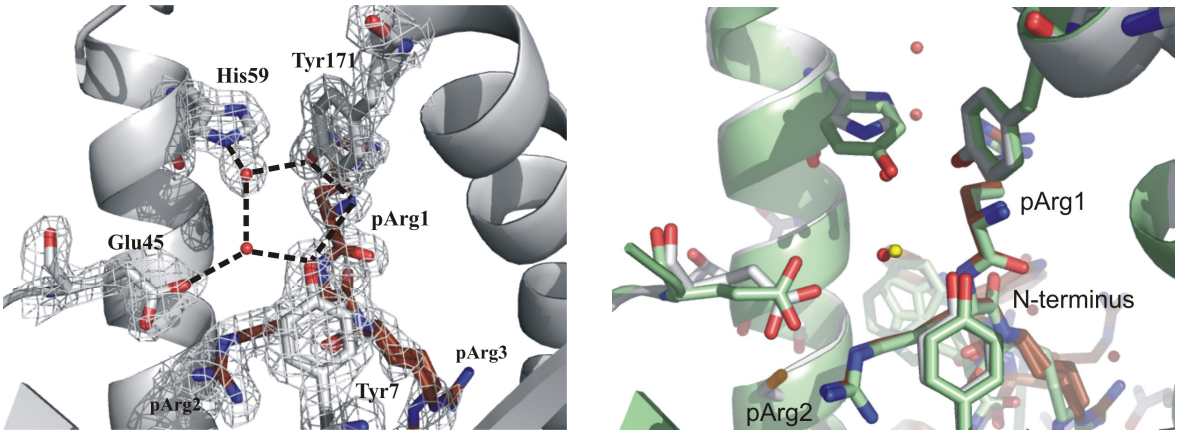

Figure 3.18. Structure of the A pocket in B*2703 subtype in complex with peptide pLMP2. a) The electron density in the A-pocket of the B*2703:β_2m:pLMP2 crystal structure. The hydrogen bonding network between conserved residues, water molecule and the carbonyl oxygen of pArg1 is marked with dashed lines, α1- and α2-helicies are in ribbon representation; b) overlay of B*2705:β_2m:pLMP2 (pale green) and B*2703:β_2m:pLMP2 (gray) showing the A pocket and the N-terminus of the peptide. The red spheres represent water molecules in B*2703:β_2m:pLMP2 structure, the yellow sphere is a strategically located water molecule in B*2705:β_2m:pLMP2.

The imidazole of His59 occupies a position similar to that of the benzene ring of Tyr59. The phenolic oxygen of Tyr59 is replaced by an additional water molecule in B*2703. This water molecule bridges His59NE (2.33 Å) and the N-terminus of pArg1 through Tyr171OH (2.66 Å), (Table 3.2). The arrangement of the imidazole moiety of His59 and its

complementation by an additional water molecule allows to maintain the characteristic pentagonal hydrogen-bonded network (Figure 3.18).

3.3.1.1.1 Thermodynamic behaviour of B*2703:pLMP2 and B*2703:pVIPR complexes

It has been already shown that a combination of structural and thermodynamic studies may aid in explaining the association of certain HLA-B27 subtypes with AS (Rudolph et al, 2002; Uchanska-Ziegler et al., 2003; Ziegler et al., 2008). The thermostabilities of HLA-B*2703 complexes with the self-peptide pVIPR and the viral peptide pLMP2 were analyzed in order to check whether thermodynamic properties of complexes are affected by the His59Tyr exchange. Since in B*2703 the amino acid sequence is changed in the A pocket, where the peptide N-terminus is anchored, I suspected to observe different thermostability of self- and viral peptide in this HLA subtype as compared to B*2705. CD and DSC measurements, performed by co-worker Dr. Rolf Misselwitz in cooperation with Dr K. Welfle and Prof. H. Welfle from the AG Biopolymerspektroskopie, Max-Delbrück Center of Molecular Medicine, Berlin-Buch, were used for all thermodynamic experiments.

A comparison of the CD melting profiles of B*2703 subtype in complex with pLMP2 and pVIPR revealed that the bound peptide has an influence on the thermostability of the whole complex (Figure 3.19).

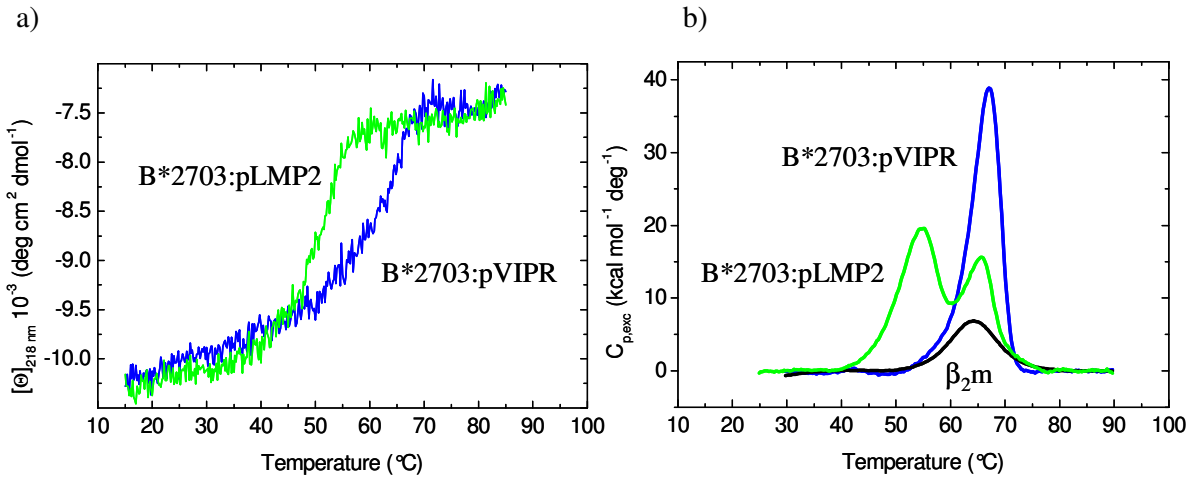

Figure 3.19. Thermal-induced unfolding of B*2703 subtype in complex with a self- and a viral peptide measured by CD and DSC. Changes of the circular dichroism were obtained at 218 nm of B*2703:β_2m:LMP2 and B*2703:β_2m:VIPR. a) The melting profile of B*2703:β_2m:pLMP2 complex indicates that 50 % of complex lost its secondary structure at lower temperature (T_m about 51.4°C) than B*2703:β_2m:pVIPR (T_m about 62.3°C), b) Experimental excessive heat capacity curves of B*2703:β_2m:pLMP2 (green line), B*2703:β_2m:VIPR (blue line) and β_2m (black line).

The complex of B*2703 with pVIPR is much more stable than the complex of the same subtype with pLMP2 (T_m values 62.3°C and 51.4°C, respectively), (Figure 3.19 a).

The DSC experiments confirmed the CD observations regarding altered thermostabilities of the complexes. Additionally, they suggested the presence of distinct unfolding patterns for complexes of B*2703 with the self- and viral peptides. The experimental DSC melting profiles of the B*2703 subtype with pVIPR showed one peak with a slight asymmetry of the transition curves on the low temperature side (Figure 3.19 b). In comparison, the DSC melting curve of B*2703:pLMP2 complex is characterized by two resolved peaks (Figure 3.19 b). β_2m unfolds in one symmetric peak as expected for small globular proteins (Figure 3.19 b). For β_2m a simple two-state unfolding pattern with a T_m of 63.8 °C was previously established (Hillig et al., 2004) (Figure 3.19 b).

To prove the reversibility of folding, β_2m and the complexes were cooled to 20°C and heated again to 90°C. About 70 % of reversibility was found for β_2m, whereas all HLA-complexes did not refold. The melting curves after the second run showed only the peak of β_2m (not shown).

3.3.1.2 Features of B*2704 in complex with pLMP2 and pVIPR

The crystals of B*2704 diffracted to 1.9 Å (B*2704:β_2m:pLMP2) or to 1.6 Å (B*2704:β_2m:pVIPR) resolution and were isomorphous; space group $P2_12_12_1$ (Table 3.3). This space group was previously found in several other complexes: B*2705 and B*2709 in complex with the m9 (Hülsmeyer et al., 2002) and TIS (Hülsmeyer et al., 2005) peptides, as well as for B*2703 in complex with the pLMP2 peptide.

Table 3.3 Data collection and refinement statistics of the B*2704:β_2m:pLMP2 and B*2704:β_2m:pVIPR complexes.

Subtype	**B*2704:β_2m:pLMP2**	**B*2704:β_2m:pVIPR**
Data collection		
Space group	$P2_12_12_1$	$P2_12_12_1$
Unit cell a; b; c [Å]	50.7, 82.3, 109.1	50.8, 82.2, 109.9
α; β; γ [°]	90; 90; 90	90; 90; 90
Resolution [Å] [a]	30.0 – 1.9 (1.93 - 1.90)	30.0 - 1.6 (1.63 - 1.60)
Unique reflections	36793 (1805)	61196 (2949)
Completeness	100.0 (100.0)	99.5 (97.4)
Redundancy	7.9 (7.5)	4.9 (4.8)
<I/σ(I)>	16.5 (3.5)	29.1 (4.5)
R_{sym} [a]	0.131 (0.583)	0.045 (0.391)
Refinement		
Non-hydrogen atoms	3872	4037
R_{cryst} [a, b]	0.152 (0.203)	0.155 (0.170)
R_{free} [a, c]	0.204 (0.243)	0.173 (0.218)
Heavy chain, no. of atoms / average B factor [Å^2]	2304 / 9.4	2368 / 14.7
β_2m, no. of atoms / average B factor [Å^2]	861 / 9.8	907 / 18.0
Peptide, no. of atoms / average B factor [Å^2]	102 / 8.0	100 / 16.4
Water, no. of molecules / average B factor [Å^2]	564 / 23.2	625 / 30.2
Glycerol, no. of atoms / average B factor [Å^2]	12 / 28.9	36 / 36.7
Rmsd [d] from ideal geometry, bond length [Å]	0.012	0.011
bond angles [°]	1.38	1.37

[a] values in parentheses refer to the highest resolution shell
[b] $R_{cryst} = \Sigma_h \left| F_o - F_c \right| / \Sigma F_o$ (working set, no σ cut-off applied)
[c] R_{free} is the same as R_{cryst}, but calculated on 5 % of the data excluded from refinement.
[d] Root-mean-square deviation (Rmsd) from target geometries.
All datasets were collected at the beamline ID 14-2 of the European Synchrotron Radiation Facility (ESRF) in Grenoble (France) at a wavelength of λ = 0.933 Å at 100 K.

For both crystals the electron density maps are very well defined (Figure 3.20). This allowed modeling of the heavy chain, β_2m and peptide as well as inserting many water molecules which improved final refinement statistics. Despite slight deviations in the area of the peptide, both complexes are similar (Figure 3.20).

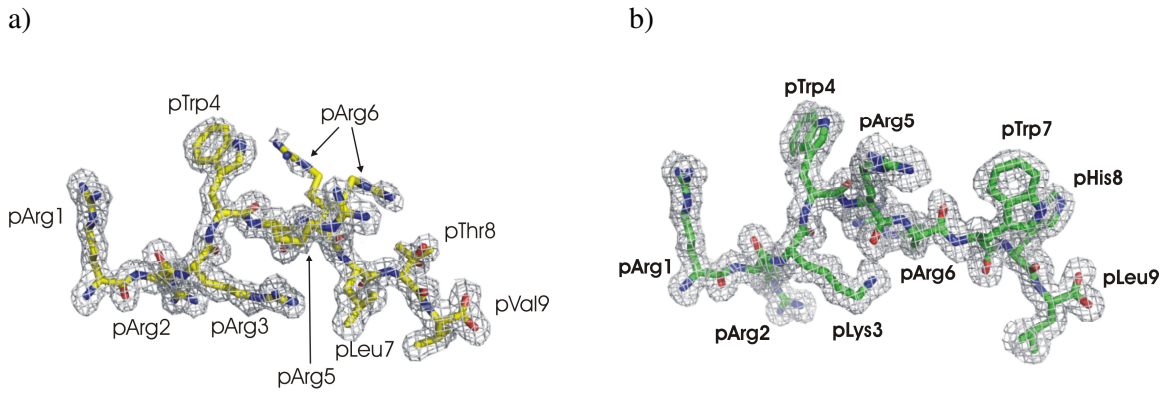

Figure 3.20. The electron densities of peptides bound to subtype B*2704. The conformation of the peptides a) pLMP2 and b) pVIPR in B*2704 viewed from the α2-helix. In both structures, pArg5 points to the viewer. The final $2F_o$-F_c electron densities are contoured at the 1 σ level.

Superposition of the two structures revealed that there are only slight differences in α1, α2 and β_2m overlays (Cα root mean square deviation of 0.475 Å). Both peptides are bound to B*2704 in a similar fashion (Cα root mean square deviation of 0.873 Å – for peptide alone). The only observed differences between B*2704 complexed with pLMP2 or pVIPR are found in the middle part, at position 4 which is a Trp in both peptides, and continue towards the C terminus of the peptide (Figure 3.20). A shift in the peptide backbone can be observed, which is most prominent at p6 (2.0 Å). High B-factors of side chains of amino acids in the middle part of both peptides indicate that this part is also more flexible (Figure 3.21).

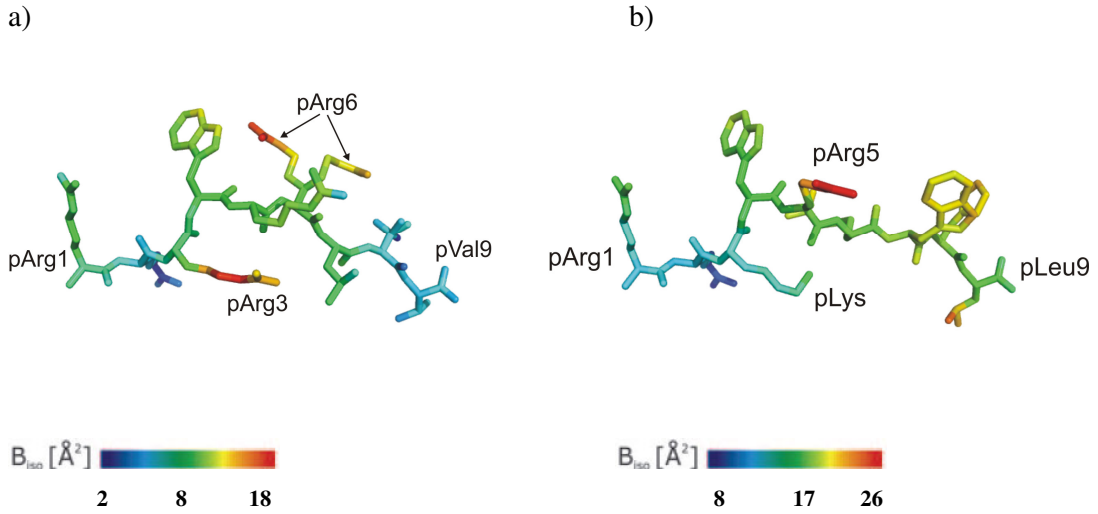

Figure 3.21. Comparison of pLMP2 and pVIPR peptide's B-factors when bound to B*2704. pLMP2 (a) and pVIPR (b) color-coded by isotropic B factor. pArg6 of pVIPR is pointing in the opposite direction than the view point, therefore it is invisible.

The Cα-atoms of the first two N terminal residues in both peptides occupy identical positions including the side chains (Figure 3.22 and Table 3.4). As in other previously described structures of HLA-B27 in complexes with these peptides, the side chain of pArg1 is sandwiched between Arg62 (α1-helix) and Trp167 (α2-helix). The C terminus looks very similar in both peptides as well, with pLeu9 of pVIPR and pVal9 of pLMP2 pointing into the binding groove. However, in the complex of pLMP2, the side chain of pVal9 inserts deeper into the binding groove of B*2704 compared with pLeu9 of pVIPR (Figure 3.22). The same situation was observed in the structure of B*2703:β_2m:pLMP2, where the two C-terminal amino acids of the peptide are localized slightly deeper in the F-pocket then in the structure of B*2703:β_2m:pVIPR.

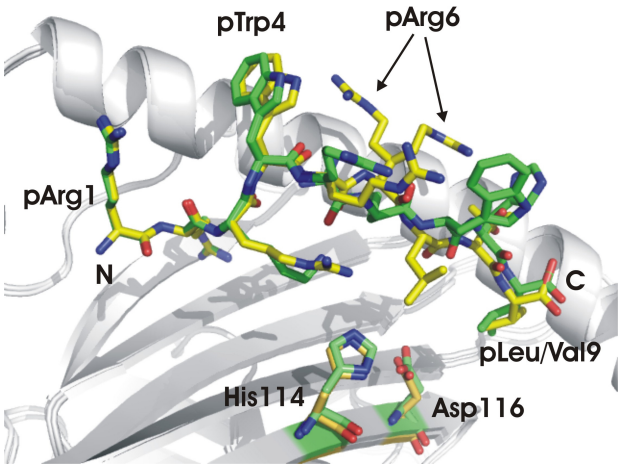

Figure 3.22. pLMP2 and pVIPR topographies when bound to B*2704 subtype. Overlay of B*2704:β_2m:pLMP2 (yellow) and B*2704:β_2m:pVIPR (green) structures. The conformation of the peptides in B*2704 is viewed from the α2-helix together with the ribbon representation of the α1-helix and the floor of the binding groove The α2-helix was removed for better visualization of the peptides.

Table 3.4 Comparison of pLMP2 and pVIPR peptide coordinations in subtype HLA-B*2704. Only direct intrapeptide contacts and contacts between peptides and HC residues are included, and solvent-mediated interactions are omitted for the sake of clarity. van der Waals' contacts are not given explicitly for each amino acid. For residues occuring in alternative conformations, only one of the equally occupied conformations is shown.

Peptide position	B*2704:β_2m:pLMP2				B*2704:β_2m:pVIPR			
	Peptide residue	**Contact residue**	**Distance [Å]**	**Interaction**	**Peptide residue**	**Contact residue**	**Distance [Å]**	**Interaction**
p1	pArg1^{N}	Tyr171^{OH}	2.6	HB	pArg1^{N}	Tyr171^{OH}	2.7	HB
	pArg1^{N}	Tyr7^{OH}	3.0	HB	pArg1^{N}	Tyr7^{OH}	3.0	HB
	pArg1^{NE}	Glu163^{OE1}	3.1	SB	pArg1^{NE}	Glu163^{OE1}	2.9	SB
	pArg1^{NH2}	Glu163^{OE1}	3.4	SB	pArg1^{NH2}	Glu163^{OE1}	3.4	SB
	pArg1^{NH2}	Glu163^{OE2}	3.3	SB	pArg1^{NH2}	Glu163^{OE2}	3.0	SB
	pArg1^{O}	Tyr159^{OH}	2.5	HB	pArg1^{O}	Tyr159^{OH}	2.7	HB
p2	Contacts formed by Arg2 are very similar in both complexes							
p3	pArg3^{N}	Tyr99^{OH}	3.0	HB	pLys3^{N}	Tyr99^{OH}	3.0	HB
	pArg3	Ile66, Tyr99, Leu156,Tyr159	3.5-4.0	vdW	pLys3	Ile66, Tyr99, Gln155, Tyr159	3.5-4.0	vdW
					pLys3^{N}	pArg5^{O}	2.7	HB
					pLys3^{O}	pArg6^{NH2}	3.3	HB
p4	The side chain of this residue is solvent-exposed in both complexes							
p5	pArg5^{NE}	Glu152^{OE1} (A)	3.1	HB	pArg5^{O}	Gln155^{NE2}	3.1	HB
	pArg5^{NE}	Glu152^{OE1} (B)	3.0	HB	pArg5	Ile66, Gln155	3.6-4.0	vdW
	pArg5^{NE}	Glu152^{OE2} (A)	3.5	HB				
	pArg5^{NE}	Gln155^{OE1} (B)	2.9	HB				
	pArg5^{NH1}	Gln155^{OE1} (B)	3.3	HB				
	pArg5^{NE2}	Gln155^{OE2}(B)	3.3	HB				
	pArg5^{NH2}	Glu152^{OE1} (B)	3.4	SB				
	pArg5^{NH2}	Gln152^{OE2} (A)	3.1	SB				
	pArg5^{NH2}	Glu152^{OE2} (B)	3.0	SB				
p6	pArg6^{NH2}	Glu76^{OE1}	2.9	SB	pArg6	Arg69, Lys70, Gln155	3.4-4.0	vdW
p7	pLeu7	Trp147, Glu152 (A)	3.5-4.0	vdW	pTrp7	Lys146, Glu152 (A), Trp147	3.4-4.0	vdW
p8	The side chain of this residue is solvent-exposed in both complexes							
	pThr8^{OG1} (B)	Ser77^{N}	3.5	HB	pHis8^{ND1}	Glu76^{OE1}	2.8	HB
	pThr8^{OG1} (B)	Ser77^{OG}	2.8	HB	pHis8^{O}	Trp147^{NE1}	3.0	HB
	pThr8^{O}	Trp147^{NE1}	2.8	HB				
	pThr8^{O}	Lys146^{NZ}	2.7	HB				
	pThr8	Glu76, Ser77, Trp147	3.8-4.0	vdW				
	pThr8^{OG1}	pVal9^{N}	3.2	HB				
p9	The side chain of this residue is buried in both complexes; the contacts formed by pVal9 in pLMP2 and pLeu9 in pVIPR are very similar							

Both pVIPR and pLMP2 are presented by the subtype B*2704 in the typical p4α conformation found in MHC class I complexes (main chain φ/Ψ torsion angles in α-helical conformation at p4) where the middle part of the peptide is exposed to the solvent. A similar peptide binding mode was previously found in the complexes B*2703:β_2m:pLMP2 and B*2709:β_2m:pLMP2 as well as in complexes of pVIPR with B*2705 and B*2709.

At p3 and p4 the backbone of the peptides is very similar and slight side chain deviations can be noticed, although both residues are pointing in the same direction. pArg5 which is

solvent-exposed in both complexes, forms a previously unobserved salt bridges in B*2704:β_2m:pLMP2 with the polymorphic residue Glu152 (Table 3.4). The highest deviations between these two peptides are seen at p6 and p7. In B*2704:β_2m:pLMP2, the side chain of pArg6 has a double conformation, although it is pointing out of the binding groove in both cases. The side chain of pArg6 of pVIPR is less solvent exposed, directed more towards the α1-helix than in case of pLMP2. However, the side chain of pArg6 in pVIPR seems to be more flexible than the pArg6 side chain of pLMP2, as indicated by higher B factors in case of pVIPR (Figure 3.21). The difference between these peptides when bound to HLA-B*2704 is also seen for p7, which in pVIPR (pTrp7) is pointing out of the groove, while pLeu7 in pLMP2 is directed towards the groove. Since T cell receptors are known to contact inter alias residue 7 of the peptide, deviations of the p7 position between self- and viral peptide might have an influence on T cell recognition. The influence of the polymorphic residue Ser77 in B*2704 is noticed in bond formation between Ser77 and amino acids of the two investigated peptides (Table 3.4). In complex with pLMP2, Ser77 interacts with pThr8 via two hydrogen bonds due to the double conformation of the pThr8 side chain, whereas in the structure of B*2704 with pVIPR there is a His at p8, and direct interaction between Ser77 and pHis8 is not possible due to the large distance (Table 3.4). However, this does not influence the overall conformation of the peptide.

3.3.1.3 Features of the B*2706 subtype in complex with pLMP2 and pVIPR

The crystals of the B*2706 subtype diffracted to 2.70 Å (B*2706:β_2m:pLMP2) or 1.83 Å (B*2706:β_2m:pVIPR) resolution. Similar to the B*2703 crystals, they were not isomorphous (Table 3.5). This is again in contrast to the B*2705 and B*2709 subtypes (space group $P2_1$, each in complex with pLMP2 and pVIPR), (Fiorillo et al., 2005) and also in contrast to B*2704, with space group $P2_12_12_1$ in complexes with both peptides.

Table 3.5 Data collection and refinement statistics of B*2706:β_2m:pLMP2 and B*2706:β_2m:pVIPR

Subtype	**B*2706:β_2m:pLMP2**	**B*2706:β_2m:pVIPR**
Data collection		
Space group	$P2_12_12_1$	$P2_1$
Unit cell a; b; c [Å]	50.7, 82.0, 108.9	50.8, 81.7, 64.43
α; β; γ [°]	90, 90, 90	90, 108, 90
Resolution [Å] [a]	30.00 – 2.70 (2.77 – 2.70)	30.00 - 1.83 (1.90 - 1.83)
Unique reflections	12253 (880)	43847 (4069)
Completeness [a]	99.0 (93.2)	99.1 (92.2)
Redundancy	2.5 (2.2)	3.6 (3.4)
$\langle I/\sigma(I)\rangle$ [a]	16.5 (3.5)	34.7 (6.0)
R_{sym} [a]	0.131 (0.583)	0.036 (0.209)
Refinement		
Non-hydrogen atoms	3333	3563
R_{cryst} [a, b]	0.190 (0.259)	0.195 (0.244)
R_{free} [a, c]	0.251 (0.352)	0.215 (0.257)
Heavy chain, no. of atoms / average B factor [Å^2]	2265 / 26.6	2340 / 23.3
β_2m, no. of atoms / average B factor [Å^2]	837 / 31.8	877 / 23.5
Peptide, no. of atoms / average B factor [Å^2]	95 / 11.9	93 / 22.2
Water, no. of molecules / average B factor [Å^2]	129 / 21.2	247 / 27.2
Glycerol, no. of atoms / average B factor [Å^2]	6 / 55.8	6 / 32.1
Rmsd [d] from ideal geometry, bond length [Å]	0.008	0.012
bond angles [°]	1.10	1.26

[a] values in parentheses refer to the highest resolution shell
[b] $R_{cryst} = \Sigma_h \left| F_o - F_c \right| / \Sigma F_o$ (working set, no σ cut-off applied)
[c] R_{free} is the same as R_{cryst}, but calculated on 5 % of the data excluded from refinement.
[d] Root-mean-square deviation (Rmsd) from target geometries.
The dataset of B*2706-pLMP2 was collected at beamline ID 14-2 of the European Synchrotron Radiation Facility (ESRF) in Grenoble (France) and that of B*2706-pVIPR at beamline BW6 of the Deutsches Elektronen-Synchrotron (DESY) in Hamburg (Germany).

Due to the high resolution of the X-ray diffraction data for the B*2706:β_2m:pVIPR complex, the electron density map was of good quality (Figure 3.23). However, it was not possible to model the side chains of peptide residues, pArg5 and pArg6. Lack of electron density is an indication that these two residues are highly flexible and disordered to such extent that the electron density is too poor to be interpreted.

In the complex B*2706:β_2m:pLMP2 it was possible to model the heavy and the light chains as well as the peptide, but due to the difference in resolution, the number of defined water molecules was much lower than in case of B*2706:β_2m:pVIPR.

a) b)

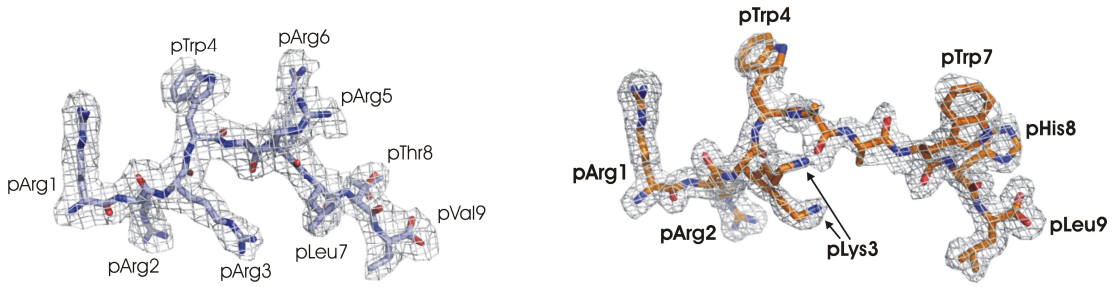

Figure 3.23. The $2F_o$-F_c electron densities of peptides bound to the B*2706 subtype. a) pLMP2 in B*2706 viewed from the α2-helix and b) pVIPR in B*2706. In B*2706:β_2m:pLMP2 structure pArg5 points to the viewer; in B*2706:β_2m:pVIPR pArg5 and pArg6 side chains are missing. The final $2F_o$-F_c electron densities are contoured at the 1 σ level and shown in blue mesh.

As for the complexes of B*2704 with the same peptides, the structures of B*2706:β_2m:pLMP2 and B*2706:β_2m:pVIPR differ only in details. Apart from the peptide, the complexes are almost identical (Cα root mean square deviation of 0.522 Å), as it was also the case in structures of other HLA-B27 subtypes. Slight differences occur only in side chains of the peptides and mostly where the amino acid is exposed to solvent. Both peptides adopt the conformation typical for a peptide bound in MHC class I molecules (p4α; Figure 3.23). The middle part of the peptide protrudes out of the binding groove, and here deviations of the backbone positions between pLMP2 and pVIPR are larger, probably due to the exposure of side chains to solvent. Side chains of these amino acids are more flexible (Figure 3.24).

a) b)

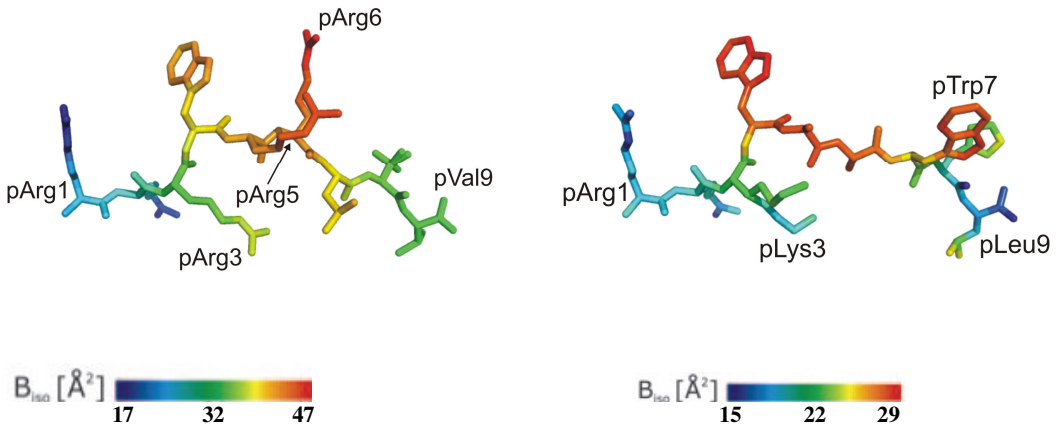

Figure 3.24. Comparison of pLMP2 and pVIPR peptide's B-factors when bound to B*2706. pLMP2 (a) and pVIPR (b) color-coded by isotropic B factor.

As already observed in other subtypes, the two N-terminal arginines of both pVIPR and pLMP2 peptides occupy identical positions within the A and B pockets respectively (Table 3.6), while there is a shift in backbone position between both peptides within and above the F pocket (Cα at p6 deviation of 2.0 Å), (Figure 3.25). A comparable difference was previously observed in the structure of B*2704 with the pVIPR and pLMP2 peptides.

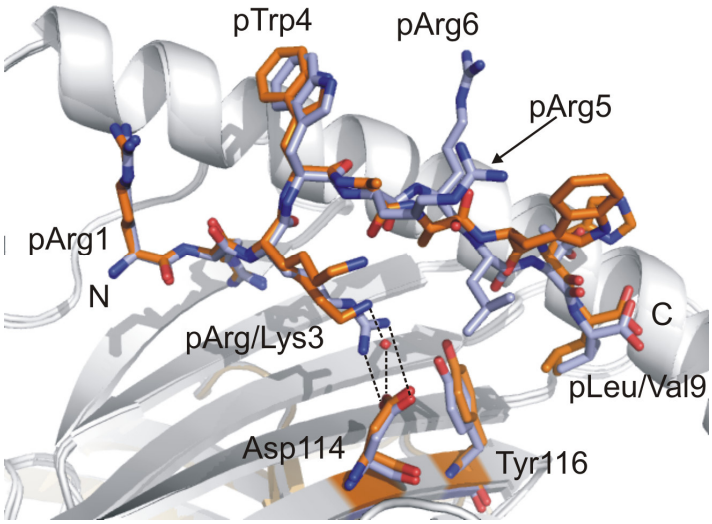

Figure 3.25. pLMP2 and pVIPR topographies when bound to the B*2706 subtype. Overlay of B*2706:β_2m:pLMP2 (blue) and B*2706:β_2m:pVIPR (orange). The conformation of the peptides is viewed from the α2-helix together with the ribbon representation of the α1-helix and the floor of the binding groove. The α2-helix was removed for better visualization of the peptides. The side chains of the polymorphic residues, Asp114 and Tyr116, are marked according to the peptide color code. The salt bridge between pArg3 and Asp114 in the B*2706:β_2m:pLMP2 and the water mediated contact between pLys3 and Asp114 in B*2706:β_2m:pVIPR structure are marked with dashed lines. The pArg5 and pArg6 side chains in the B*2706:β_2m:pVIPR structure are missing.

A significant difference was noticed at pLys3 which occurs in double conformation (pVIPR) directed towards the α2-helix. In one of the conformations, the side chain is buried deeper and forms a water-mediated hydrogen bond with Asp114 at the floor of the groove (Figure 3.25). Since the distance between this residues is larger than in case of pArg3 in pLMP2 due to the shorter side chain of pLys3, the contact is mediated by a water molecule (distance between pLys3NZ and water – 2.77 Å, between water and Asp114OD – 2.72 Å). In the viral peptide pLMP2, the third position is occupied by an arginine residue, which also points deep into the binding groove (Figure 3.25) but forms a salt bridge (2.9 Å) with Asp114 (Table 3.6).

Table 3.6 Comparison of pLMP2 and pVIPR peptides coordinations in HLA-B*2706 subtype. Only direct intrapeptide contacts and contacts between peptides and HC residues are included, and solvent-mediated interactions are omitted for the sake of clarity. van der Waals' contacts are not given explicitly for each amino acid. For residues which occur in alternative conformations only one of the equally occupied conformations is shown.

Peptide position	B*2706:β_2m:pLMP2				B*2706:β_2m:pVIPR			
	Peptide residue	**Contact residue**	**Distance [Å]**	**Interaction**	**Peptide residue**	**Contact residue**	**Distance [Å]**	**Interaction**
p1	pArg1^{N}	Tyr171^{OH}	2.8	HB	pArg1^{N}	Tyr171^{OH}	2.7	HB
	pArg1^{N}	Tyr7^{OH}	3.4	HB	pArg1^{N}	Tyr7^{OH}	3.1	HB
	pArg1^{NE2}	Glu163^{OE1}	3.5	SB	pArg1^{NE2}	Arg62^{NH1}	3.4	HB
	pArg^{NH1}	Arg62^{NE}	3.2	HB	pArg1^{NE2}	Glu163^{OE1}	2.9	SB
	pArg1^{NH2}	Glu163^{OE1}	3.5	SB	pArg1^{NH2}	Glu163^{OE1}	3.4	SB
	pArg1^{NH2}	Glu163^{OE2}	3.3	SB	pArg1^{NH2}	Glu163^{OE2}	2.8	SB
	pArg1^{O}	Tyr159^{OH}	2.5	HB	pArg1^{NH1}	Arg62^{NE}	3.7	HB
					pArg1^{O}	Tyr159^{OH}	2.7	HB
p2	Contacts formed by Arg2 are very similar in both complexes							
p3	pArg3^{N}	Tyr99^{OH}	2.9	HB	pLys3^{N}	Tyr99^{OH}	3.0	HB
	pArg3	Ile66, Tyr99, Leu156,Tyr159	3.6-4.0	vdW	pLys3	Ile66, Tyr99, Gln155, Tyr159	3.5-4.2	vdW
	pArg3^{NH2}	Asp114^{OD1}	2.9	SB	pLys3^{NZ}(B)	pArg5^{O}	3.2	HB
	pArg3^{NH}	Asn97ND	3.0	HB				
p4	The side chain of this residue is solvent-exposed in both complexes							
p5	pArg5^{NH2}	Glu152^{OE2}	3.3	SB	Side chain has not been modeled due to lack of electron density			
p6	The side chain is solvent exposed				Side chain has not been modeled due to lack of electron density			
p7	pLeu7	Trp147, Glu152	3.3-4.0	vdW	pTrp7^{N}	Glu152^{OE2}	3.2	HB
					pTrp7	Trp147, Ala150, Glu152	3.4-4.0	vdW
p8	The side chain of this residue is solvent-exposed in both complexes							
	pThr8^{OG1}(A)	Glu76^{OE2}(A)	3.5	HB	pHis8^{NE2}	Glu76^{OE2}	3.4	HB
	pThr8^{OG1}(B)	Lys146^{NZ}	3.5	HB	pHis8^{O}	Trp147^{NE1}	3.0	HB
	pThr8^{OG1}(B)	Ser77^{N}	3.6	HB	pHis8	Thr73,	3.8-4.0	vdW
	pThr8^{OG1}(B)	Ser77^{OG}	2.8	HB		Glu76(A)		
	pThr8^{O}	Trp147^{NE1}	3.0	HB				
	pThr8^{O}	Lys146^{NZ}	3.3	HB				
	pThr8	Glu76, Ser77, Trp147		vdW				
p9	The side chain of this residue is buried in both complexes; the contacts formed by pVal9 in pLMP2 and pLeu9 in pVIPR are very similar							

Both peptides are presented by the B*2706 subtype in the typical conformation with amino acids of the middle part exposed to solvent. The pTrp4 in both structures is solvent exposed and assumes a similar position. Although it was not possible to model side chains of pArg5 and pArg6 of pVIPR, the positions of the Cα atoms indicate that the peptide adopts the p4α conformation. In case of pLMP2, pArg5 and pArg6 are solvent exposed, similar to the structures of B*2709:β_2m:pLMP2 (Fiorillo et al., 2005) and B*2703:β_2m:pLMP2. pArg5 in B*2706:β_2m:pLMP2 forms a salt bridge with the polymorphic Glu152 (3.3 Å) (Table 3.6) similar to what has already been observed in the structure of B*2704:β_2m:pLMP2. A major

difference between these two peptides, when bound to B*2706, can be seen at p7, since pLeu7 from pLMP2 is pointing to the floor of the groove, whereas pTrp7 in pVIPR is solvent-exposed and pulls up the backbone. The C-terminus is therefore slightly closer to the α1-helix. The shift in backbones is most pronounced at p7 which might explain side chains rearrangements. In the pLMP2 peptide, pThr8 side chain occurs in two conformations, whereas for pVIPR the side chain of pLys3 in two conformations was observed. The effect of Asp77 to Ser77 exchange is similar as in the B*2704 subtype. Ser77 contacts both conformations of peptide residue pThr8 via two hydrogen bonds, but no interaction between pHis8 and Ser77 was observed. As in B*2704 the polymorphic residue at position 77 does not affect the peptide conformation.

3.3.2 Structural comparison of pLMP2 and pVIPR binding modes when complexed to different HLA-B27 subtypes

With five different subtypes (B*2703/04/05/06/09), each in complex with two different peptides (pLMP2 and pVIPR), we have in our hands a repertoire of crystal structures of the complexes, which permits a detailed analysis and comparison of peptide presentation within the different HLA-B27 molecules. It allows also to verify whether molecular mimicry, which has been proposed for B*2705 and B*2709, is also present in B*2704 and B*2706.

3.3.2.1 Comparative analysis of B*2704 and B*2706 complexed with a self- and a viral peptide

HLA-B*2704 and HLA-B*2706 are known to be closely related to each other but also differently associated with the autoimmune disease Ankylosing Spondylitis. Since previous experiments with B*2705 and B*2709 had suggested the existence of molecular mimicry between these differently AS-associated subtypes (Fiorillo et al., 2005), the comparison of peptide presentation by B*2704 and B*2706 may aid in understanding a role of self- and viral peptides in this autoimmune disorder and verify whether molecular mimicry might explain AS pathogenesis.

As expected from the peptide sequences, the binding modes of pLMP2 and pVIPR are most similar near the N-terminus. This has already been seen in other described to date structures of HLA-B27 complexed with the viral peptide. The arginine residues at position p1 and p2 are in

identical positions in complexes of pLMP2 and pVIPR with both subtypes. Minor differences are seen in p3 and p9 side chains conformations (Figure 3.26).

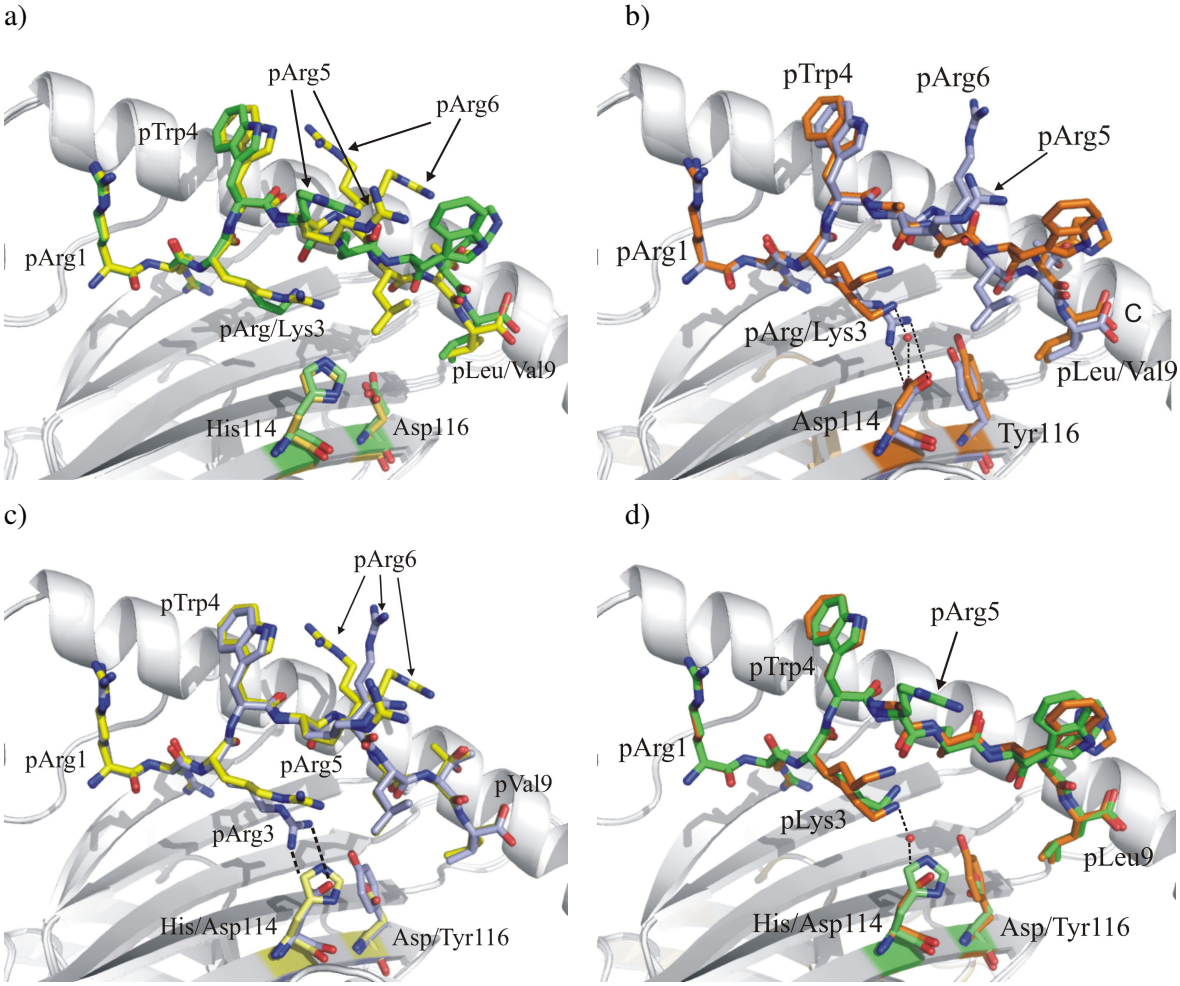

Figure 3.26. Structural comparison of pLMP2 and pVIPR as presented by B*2704 and B*2706 subtypes. Structures overlay of a) B*2704:β_2m:pLMP2 (yellow) and B*2704:β_2m:pVIPR (green), b) B*2706:β_2m:pLMP2 (blue) and B*2706:β_2m:pVIPR (orange), c) B*2704:β_2m:pLMP2 (yellow) and B*2706:β_2m:pLMP2 (blue), d) B*2704:β_2m:pVIPR (green) and B*2706:β_2m:pVIPR (orange). All structures are in p4α conformation. The conformation of the peptides in B*2704 is viewed from the α2-helix together with the ribbon representation of the α1-helix and the floor of the binding groove The α2-helix was removed for better visualization of the peptides. The side chains of the polymorphic residues His/Asp114 and Asp/Tyr116 are marked according to the peptide color code. The salt bridge between pArg3 and Asp114 in the B*2706:β_2m:pLMP2 and the water mediated contact between pLys3 and Asp114 in B*2706:β_2m:pVIPR structure are marked with dashed lines. pArg5 and pArg6 side chains in B*2706:β_2m:pVIPR structure are missing.

The backbones of the pLMP2 and pVIPR peptides are in almost identical positions in B*2704 and in B*2706 (Cα root mean square deviation of 0.150 Å for p1-p9 of the pLMP2 peptide and 0.256 Å for p1-p9 of the pVIPR peptide) The only discrepancies between the two structures can be seen in side chain conformations of some amino acids (Figure 3.26). This starts in B*2706 at p3, where part of the side chain of pArg3 in pLMP2 and pLys3 in pVIPR inserts deeper into the binding groove. This feature is observed for the first time here, and pArg3 in case

of pLMP2 is thus established as a secondary anchor residue due to a salt bridge formation to the polymorphic Asp114 (Figure 3.26 and Table 3.6 from section 3.3.1.3). The amino acids in the middle part of both peptides are solvent exposed, and the only difference can be seen in side chains arrangement (Figure 3.26).

In the structures of B*2704:β_2m:pLMP2 and B*2706:β_2m:pLMP2, pArg5 takes slightly different position than in the complex of B*2704 with pVIPR, and interacts with the polymorphic residue Glu152 via a salt bridge (Table 3.4 and Table 3.6 in sections 3.3.1.2 and 3.3.1.3). Since Glu152 is localized in the α2-helix, pArg5 is pointing in its direction (Figure 3.26). As a consequence, the pLMP2 peptide adopts the p4α conformation.

In the peptide C-termini, the positions of amino acids show again high similarity in complexes with both subtypes. Even the effect of the two other polymorphic residues (with respect to the ancestral allele B*2705) which are located outside the floor of the binding groove is the same in B*2704 and B*2706. Ser77 contacts pThr8 of pLMP2 via hydrogen bonds and the distances are of similar length. The interaction between the amino acid at position 77 and pThr8 of the pLMP2 peptide has been observed neither in B*2703, nor in the previously investigated B*2705 and B*2709 subtypes. In case of the pVIPR peptide, pHis8 is not able to interact directly with Ser77 due to a shorter side chain, and the imidazole ring of the pHis8 is located in a slightly different position than in the structures described so far, however, it does not change the overall peptide binding mode. Gly211, present in the α3-helix, does not contact the peptide residues directly and seems not to influence the peptide conformation at all.

In conclusion, despite of two amino acids difference in the floor of the binding groove between B*2704 and B*2706, the binding mode of the viral- and the self peptide in these subtypes is extremely similar.

3.3.2.2 Structural analysis of the pLMP2 binding mode in complexes with B*2703, B*2704, B*2705, B*2706 and B*2709

The crystal structures of B*2705/09:β_2m:pLMP2 (Fiorillo et al., 2005) have previously been solved crystallizing in space group $P2_1$. In contrast, B*2703:β_2m:pLMP2 crystallized in space group $P2_12_12_1$ (Table 3.1), and the same space group has been observed in complexes of pLMP2 with B*2704 and B*2706 (Table 3.3 and 3.5). Comparison of the structures of pLMP2 in complexes with B*2703/04/05/06/09 brought unexpected results. From the X-ray structures carried out earlier it was concluded that the AS-associated B*2705 subtype presents the viral

peptide pLMP2 in a drastically different fashion than B*2709 (which is not associated with the disease), (Fiorillo et al., 2005). This is clearly due to the Asp116His exchange in the binding groove.

The B*2704 subtype is also disease associated and differs from the ancestral B*2705 subtype in three amino acids that are located on α1-, α2-helix or within the α3-domain. The floor of the binding groove of B*2704 and B*2703 is conserved with respect to the amino acid sequence compared with the B*2705 subtype. The conformation of the pLMP2 peptide in complex with B*2705 was determined to be in p6α conformation, with pArg5 forming a salt bridge to Asp 116 in the groove. Since the binding grooves in B*2705, B*2703 and B*2704 are similar, I expected to find binding of the pLMP2 peptide in the p6α conformation (as in B*2705) as well. Surprisingly, the pLMP2 peptide in B*2703 and B*2704 adopts the p4α conformation, which was found for this peptide so far only in B*2709 (Figure 3.27 and 3.28).

a)

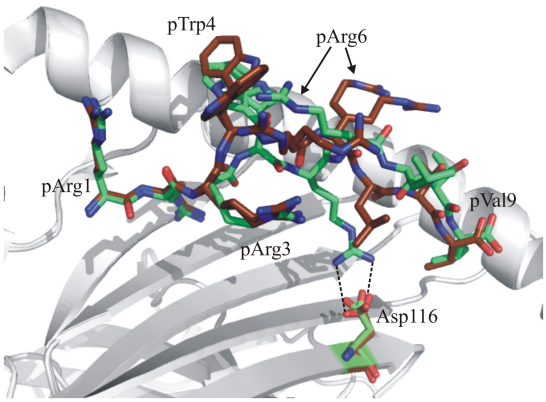

b)

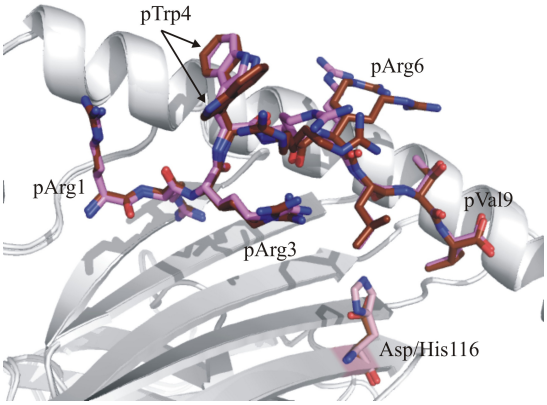

c)

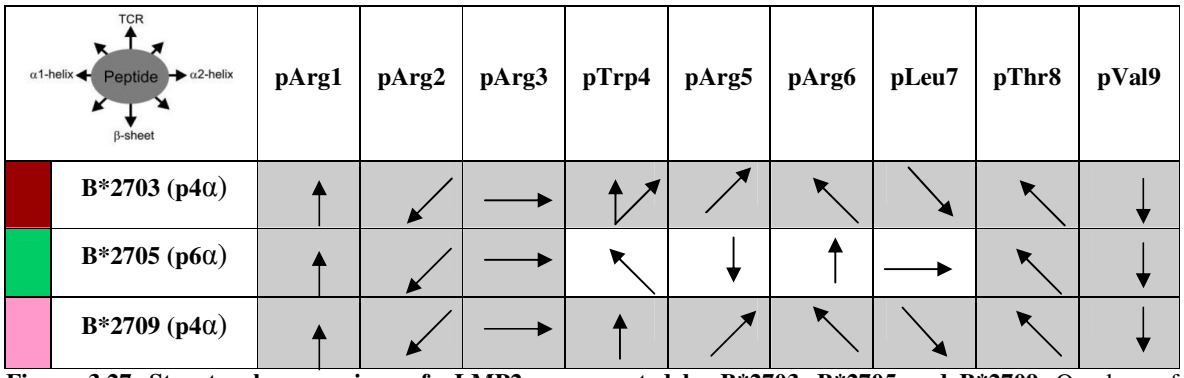

Figure 3.27. Structural comparison of pLMP2 as presented by B*2703, B*2705 and B*2709. Overlays of structures: a) B*2705:β_2m:pLMP2 (green) in p6α conformation and B*2703:β_2m:pLMP2 (brown) in p4α, b) B*2709:β_2m:pLMP2 (pink) and B*2703:β_2m:pLMP2 (brown) both in p4α conformation. The view point is from the α2-helix, which was removed for better visualization. The polymorphic residues Asp116 (in B*2703 and B*2705) or His116 (in B*2709) are colored according to the peptide color code. The salt bridge between pArg5 and Asp116 in B*2705:β_2m:pLMP2 structure is marked with dashed lines, c) Schematic diagram showing the side chains orientations of pLMP2 peptide in B*2703, B*2705 and B*2709 binding groove. The *shaded areas* indicate structural similarity between the pLMP2 peptide as presented by B*2703, B*2705, and B*2709. For pTrp4 of pLMP2 in B*2703, a double conformation was found.

a)

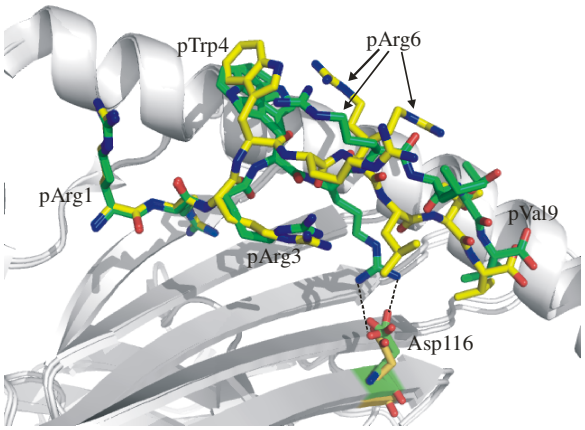

b)

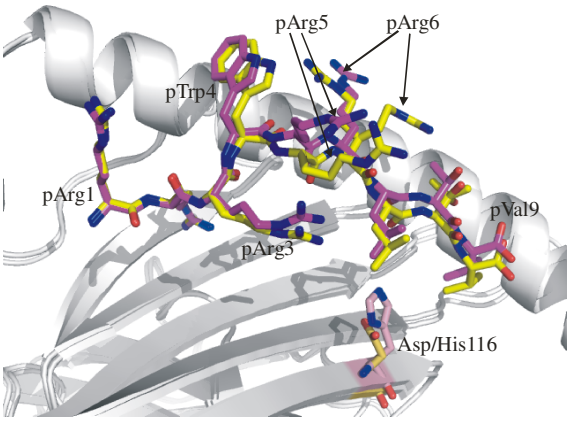

c)

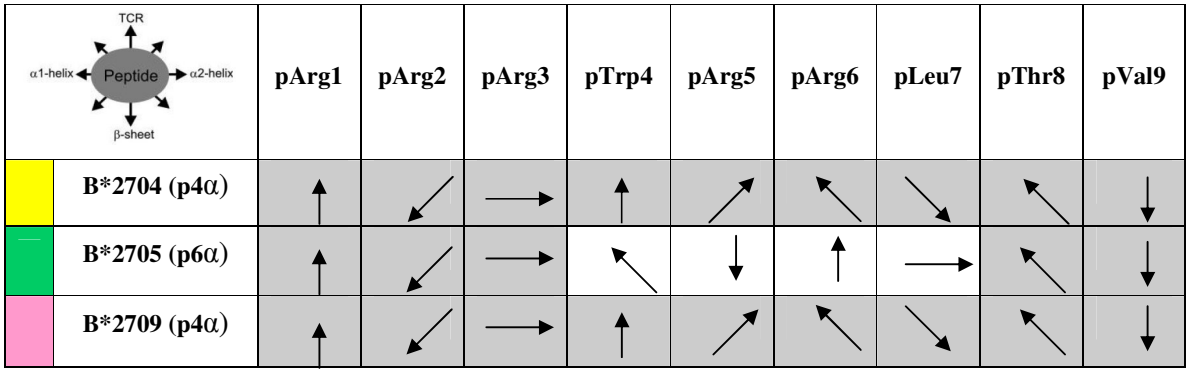

Figure 3.28. Structural comparison of pLMP2 as presented by B*2704, B*2705 and B*2709 Comparison of crystal structures of a) B*2704:β_2m:pLMP2 (yellow) with B*2705:β_2m:pLMP2 (green) and b) B*2704:β_2m:pLMP2 (yellow) with B*2709:β_2m:pLMP2 (pink). The view point is from the α2-helix, which was removed for better visualization. The side chain of the polymorphic residue, Asp116 in B*2705 and in B*2704 or His116 in B*2709 is marked according to the peptide color code. The salt bridge between pArg5 and Asp116 in the B*2705:β_2m:pLMP2 structure is drawn in black with dashed lines. The salt bridge between Glu152 and pArg5 in B*2704:β_2m:pLMP2 is not shown. c) Schematic diagram showing the side chains orientations of pLMP2 peptide in B*2704, B*2705 and B*2709 binding groove. The *shaded areas* indicate structural similarity between the pLMP2 peptide as presented by B*2704, B*2705, and B*2709.

The subtype B*2706 differs from the ancestral HLA subtype B*2705 as well as from B*2709 in five residues. They are located either at the bottom of the binding groove or reside in the α1- and α2-helix or within the α3-domain. It could be expected that the His114Asp exchange will have an influence on the peptide binding mode as in case of B*2705 and B*2709, where the single exchange at position 116 from Asp in B*2705 to His in B*2709 caused a conformational change in peptide presentation by these subtypes. However, in case of pLMP2 binding to B*2706, the classical p4α peptide conformation with pArg5 exposed to the solvent was observed (Figure 3.29). The mode of peptide binding is therefore most similar to B*2703, B*2704 and B*2709 subtypes.

a)

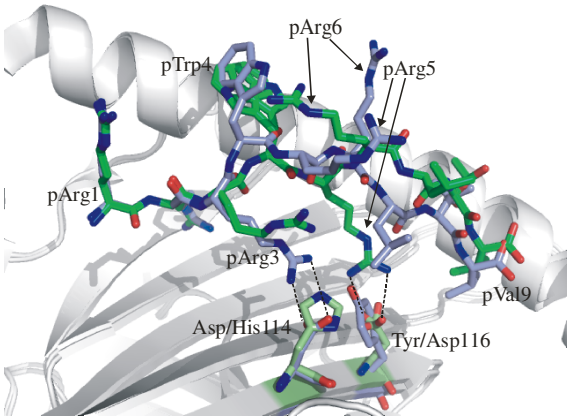

b)

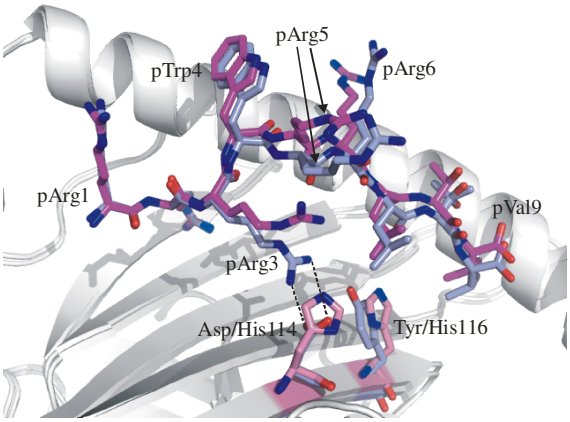

c)

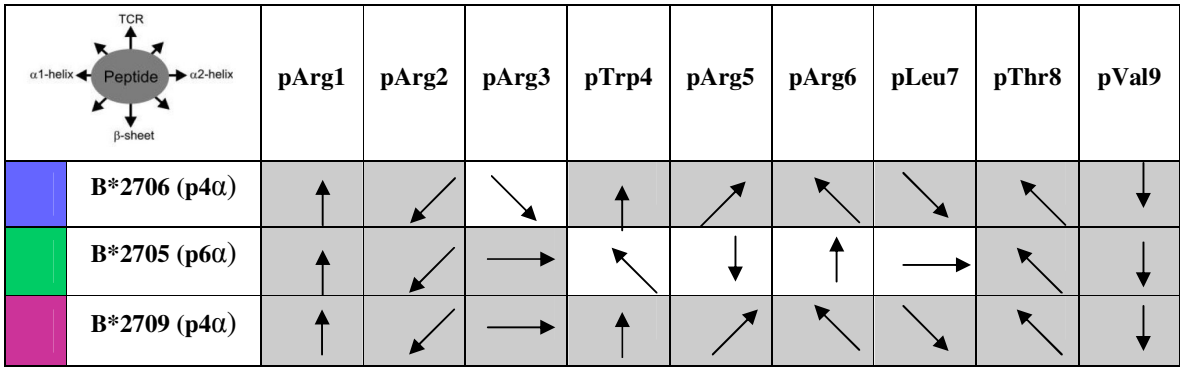

Figure 3.29. Structural comparison of pLMP2 as presented by B*2706, B*2705 and B*2709. Comparison of crystal structures of a) B*2706:β_2m:pLMP2 (blue) with B*2705:β_2m:pLMP2 (green) and b) B*2706:β_2m:pLMP2 (blue) with B*2709:β_2m:pLMP2 (violet). The view point is from the α2-helix, which was removed for better visualization. The side chain of the polymorphic residues, Asp114 and Tyr116 in B*2706, His114 and Asp116 in B*2705 or His114 and His116 in B*2709, are marked according to the peptide color code. The salt bridges between pArg3 and Asp114 in B*2706:β_2m:pLMP and between pArg5 and Asp116 in B*2705:β_2m:pLMP2 are indicated with dashed lines, c) Schematic diagram showing the side chains orientations of pLMP2 peptide in B*2706, B*2705 and B*2709 binding groove. The *shaded areas* indicate structural similarity between the pLMP2 peptide as presented by B*2706, B*2705, and B*2709.

Even when looking at details we can say that all structures discussed here are similar (Table 3.7, and Table 3.8). The residues p1 and p2 exhibit identical positions in all compared subtypes (Figure 3.27, 3.28, 3.29 and 3.30) and the side chains of the amino acids p3 and p9 show only negligible variations with exception of B*2706 where the pArg3 inserts deeper in the binding groove and contacts Asp114 via salt bridge. Even the polymorphism at position 59 in B*2703 subtype does not influence the positioning of pArg1, since the pentagonal bonding network within A-pocket remains unchanged due to an additional water molecule in this area (Figure 3.27 and 3.30).

a)

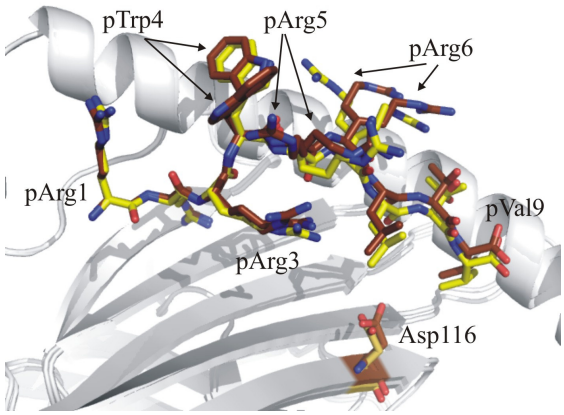

b)

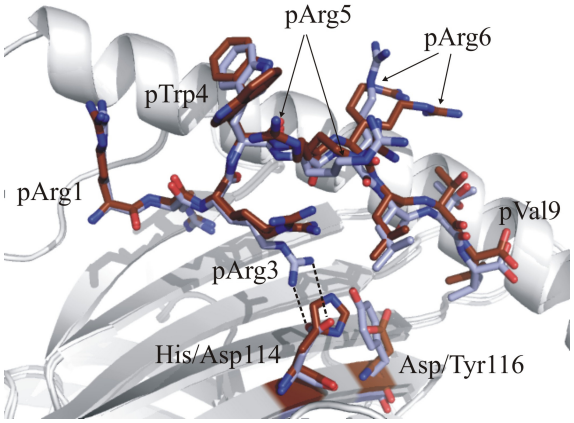

c)

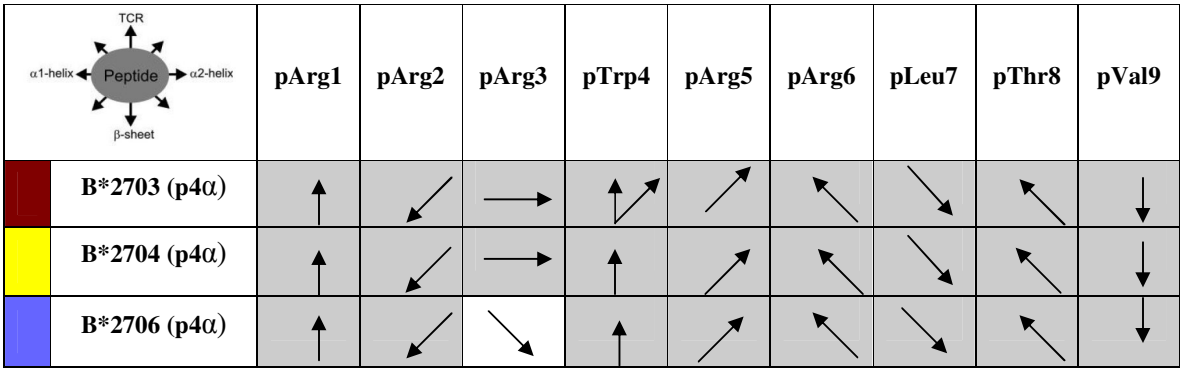

Figure 3.30. Structural comparison of pLMP2 as presented by B*2703, B*2704 and B*2706. Comparison of crystal structures of a) B*2704:β_2m:pLMP2 (yellow) and B*2703:β_2m:pLMP2 (brown), both in p4α conformation, b) B*2706:β_2m:pLMP2 (blue) and B*2703:β_2m:pLMP2 (brown), both in p4α conformation. The view point is from the α2-helix, which was removed for better visualization. The side chains of the polymorphic residues are marked according to the peptide color code. The salt bridge between pArg3 and Asp114 in B*2706:β_2m:pLMP is indicated with dashed lines. c) Schematic diagram showing the side chains orientations of pLMP2 peptide in B*2703, B*2704 and B*2706 binding groove. The *shaded areas* indicate structural similarity between the pLMP2 peptide as presented by B*2703, B*2704, and B*2706.

The backbone of the peptide in complexes with B*2703, B*2704, B*2706 and B*2709 is also similar in the middle part (Table 3.8); however, the side chains deviations between these subtypes are more pronounced here probably as a consequence of their exposure to the solvent. Starting with residue pTrp4, the backbone of pLMP2 in B*2703/B*2704/B*2706 reveals a different conformation than in the subtype B*2705 but it resembles the binding mode of pLMP2 in B*2709 (Figure 3.27, 3.28 and 3.29). Although the side chain of p4 in all compared structures is solvent-exposed, it is directed more towards the α1 helix in B*2705 (Figure 3.28 c).

Table 3.7 Comparison of pLMP2 peptide coordination in the B*2703, B*2704, B*2706 and B*2705 subtypes. Only direct intrapeptide contacts and contacts between pLMP2 and HC residues are included, and solvent-mediated interactions are omitted. van der Waals' contacts are not given explicitly for each amino acid. Interactions for B*2705 are taken from Fiorillo et al., 2005

Peptide position	B*2703:β_2m:pLMP2				B*2704:β_2m:pLMP2				B*2706:β_2m:pLMP2				B*2705:β_2m:pLMP2			
	Peptide residue	**Contact residue**	**Dist [Å]**	**Interaction**	**Peptide residue**	**Contact residue**	**Dist [Å]**	**Interaction**	**Peptide residue**	**Contact residue**	**Dist [Å]**	**Interaction**	**Peptide residue**	**Contact residue**	**Dist [Å]**	**Interaction**
pArg1 **pArg2** **pArg3**	Contacts formed by pArg1, pArg2 and pArg3 are very similar in all complexes															
pTrp4	Solvent-exposed				Solvent-exposed				Solvent-exposed				Solvent-exposed			
	pTrp4O pTrp4	pArg6^{N} Arg62 Gln65, Ile66	3.4 3.6-4.0	HB vdW	No direct contact to peptide or HC residues				No direct contact to peptide or HC residues				pTrp4	pArg6 Ile66 (B)	~3.3 -3.5 ~3.5 -3.7	vdW vdW
pArg5	Solvent-exposed				Solvent-exposed				Solvent-exposed				Burried			
	pArg5^{ND1}(A) pArg5^{NE2}	pArg3^{NH2}(A) Gln155^{OE1}	2.9 2.8	HB HB	pArg5^{NH2} pArg5^{NH2} pArg5^{NH2}	Glu152^{OE1} (B) Gln152^{OE2} (A) Gln152^{OE2} (B)	3.4 3.1 3.0	SB SB SB	pArg5^{NH2}	Glu152^{OE2}	3.3	SB	pArg5^{NH1} pArg5^{NH2}	Asp116^{OD1} Asp116^{OD2}	3.13 2.98	SB SB
pArg6	Solvent-exposed				Solvent-exposed				Solvent-exposed				Solvent-exposed			
	pArg6^{NH1} B	Glu76^{OE1} A	3.0	SB	pArg6^{NH2}	Glu76^{OE1}	2.9	SB	No direct contact to peptide or HC residues				pArg6	pTrp4	~3.3 -3.5	vdW
pLeu7	Burried				Burried				Burried				Solvent-exposed			
	pLeu7	His114, Trp147	~3.5	vdW	pLeu7	Trp147, Glu152 (A)	3.5-4.0	vdW	pLeu7	Trp147, Glu152	3.3-4.0	vdW	pLeu7	Val152	~3.5	vdW
pThr8	Solvent-exposed				Solvent-exposed				Solvent-exposed				Solvent-exposed			
	pThr8^{OG1} pThr8^{O} pThr8^{O} pThr8	Lys146^{NZ} Lys146^{NZ} Trp147^{NE1} Glu76, Asp77	2.8 2.9 2.9	HB HB HB vdW	pThr8^{OG1} (B) pThr8^{OG1} (B) pThr8^{O} pThr8^{O} pThr8 pThr8^{OG1}	Ser77^{N} Ser77^{OG} Trp147^{NE1} Lys146^{NZ} Glu76, Ser77, Trp147 pVal9^{N}	3.5 2.8 2.8 2.7 3.8 -4.0 3.2	HB HB HB HB vdW HB	pThr8^{OG1}(A) pThr8^{OG1}(B) pThr8^{OG1}(B) pThr8^{OG1}(B) pThr8^{O} pThr8^{O} pThr8	Glu76^{OE2}(A) Lys146^{NZ} Ser77^{N} Ser77^{OG} Trp147^{NE1} Lys146^{NZ} Glu76, Ser77, Trp147	3.5 3.5 3.6 2.8 3.0 3.3	HB HB HB HB HB HB vdW	pThr8^{OG1} pThr8^{O}	Lys146^{NZ} Lys146^{NZ} Trp147^{NZ}	2.7 3.2 3.0	HB HB HB
pVal9	pVal9^{N}	Asp77^{OD1}	3.0	HB	pVal9^{NH}	Ser77^{OH}	3.1	HB	pVal9^{NH}	Ser77^{OH}	3.2	HB	pVal9^{N}	Asp77^{OD1}	2.8	HB

Table 3.8 Comparison of pLMP2 peptide coordination in the B*2703, B*2704, B*2706 and B*2709 subtypes. Only direct intrapeptide contacts and contacts between pLMP2 and HC residues are included, and solvent-mediated interactions are omitted. van der Waals' contacts are not given explicitly for each amino acid. Interactions for B*2709 are taken from Fiorillo et al., 2005.

Peptide position	B*2703:β_2m:pLMP2				B*2704:β_2m:pLMP2				B*2706:β_2m:pLMP2				B*2709:β_2m:pLMP2			
	Peptide residue	**Contact residue**	**Dist [Å]**	**Interaction**	**Peptide residue**	**Contact residue**	**Dist [Å]**	**Interaction**	**Peptide residue**	**Contact residue**	**Dist [Å]**	**Interaction**	**Peptide residue**	**Contact residue**	**Dist [Å]**	**Interaction**
pArg1 **pArg2** **pArg3**	Contacts formed by pArg1, pArg2 and pArg3 are very similar in all complexes															
pTrp4	Solvent-exposed				Solvent-exposed				Solvent-exposed				Solvent-exposed			
	pTrp4O pTrp4	pArg6^{N} Arg62 Gln65, Ile66	3.4 3.6-4.0	HB vdW	No direct contact to peptide or HC residues				No direct contact to peptide or HC residues				No direct contact to peptide or HC residues			
pArg5	Solvent-exposed				Solvent-exposed				Solvent-exposed				Solvent-exposed			
	pArg5^{ND1}(A) pArg5^{NE2}	pArg3^{NH2}(A) Gln155^{OE1}	2.9 2.8	HB HB	pArg5^{NH2} pArg5^{NH2} pArg5^{NH2}	Glu152^{OE1} (B) Gln152^{OE2} (A) Gln152^{OE2} (B)	3.4 3.1 3.0	SB SB SB	pArg5^{NH2}	Glu152^{OE2}	3.3	SB	No direct contact to peptide or HC residues			
pArg6	Solvent-exposed				Solvent-exposed				Solvent-exposed				Solvent-exposed			
	pArg6^{NH1} B	Glu76^{OE1} A	3.0	SB	pArg6^{NH2}	Glu76^{OE1}	2.9	SB	No direct contact to peptide or HC residues				pArg6^{NH1} pArg6	Glu72^{OE1} Ala69^{NE2}	3.1 3.6	SB vdW
pLeu7	Burried				Burried				Burried				Burried			
	pLeu7	His114, Trp147	~3.5	vdW	pLeu7	Trp147, Glu152 (A)	3.5-4.0	vdW	pLeu7	Trp147, Glu152	3.3-4.0	vdW	pLeu7	Trp147 Val152	3.6-3.7 3.6-3.7	vdW vdW
pThr8	Solvent-exposed				Solvent-exposed				Solvent-exposed				Solvent-exposed			
	pThr8^{OG1} pThr8^{O} pThr8^{O} pThr8	Lys146^{NZ} Lys146^{NZ} Trp147^{NE1} Glu76, Asp77	2.8 2.9 2.9	HB HB HB vdW	pThr8^{OG1} (B) pThr8^{OG1} (B) pThr8^{O} pThr8^{O} pThr8 pThr8^{OG1}	Ser77^{N} Ser77^{OG} Trp147^{NE1} Lys146^{NZ} Glu76, Ser77, Trp147 pVal9^{N}	3.5 2.8 2.8 2.7 3.8 - 4.0 3.2	HB HB HB HB vdW HB	pThr8^{OG1}(A) pThr8^{OG1}(B) pThr8^{OG1}(B) pThr8^{OG1}(B) pThr8^{O} pThr8^{O} pThr8	Glu76^{OE2}(A) Lys146^{NZ} Ser77^{N} Ser77^{OG} Trp147^{NE1} Lys146^{NZ} Glu76, Ser77, Trp147	3.5 3.5 3.6 2.8 3.0 3.3	HB HB HB HB HB HB vdW	pThr8^{OG1} pThr8^{O} pThr8^{O}	Lys146^{NZ} Lys146^{NZ} Lys146^{NZ} Trp147^{NZ}	2.7 3.2 2.9 2.8	HB HB HB HB
pVal9	pVal9^{N}	Asp77^{OD1}	3.0	HB	pVal9^{NH}	Ser77^{OH}	3.1	HB	pVal9^{NH}	Ser77^{OH}	3.2	HB	pVal9^{N}	Asp77^{OD1}	2.8	HB

In B*2703, B*2704, and B*2706 residue p5 is solvent exposed as it was in B*2709:β_2m:pLMP2 (Figure 3.27, 3.28 and 3.29). In comparison, the peptide conformation in B*2705 adopts a drastically different binding mode with pArg5 pointing into the groove (Figure 3.28 a and c) that enables salt bridge formation with Asp116 (Table 3.7). This causes apparently a change in conformation of both side chain and backbone of pArg6. In all five subtypes pArg6 is solvent-accessible, however in B*2703/04/09 it makes a few contacts to the α1-helix, whereas in B*2705 it is pointing in different direction than in B*2703/04/06/09 and forms intrapeptide connection to pTrp4 (Table 3.7 and Table 3.8).

A significant change is seen between B*2706 and B*2705 in the middle part of pLMP2 peptide conformation (Figure 3.29). Instead of the salt bridge between Asp116 and pArg5 which occurs in B*2705:β_2m:pLMP2, in B*2706:β_2m:pLMP2 a salt bridge (2.9 Å) is formed between Asp114 and pArg3 (Table 3.6 in section 3.3.1.3). Asp114 which is already occupied can not form contact to pArg5 which might explain the peptide conformation in B*2706.

The side chain of the p5 residue in the B*2704 and B*2706 subtypes takes slightly different position than in B*2709 and B*2703. This can be explained by the Val152Glu substitution in α2 helix which causes formation of a novel salt bridge between pArg5NH2 and Glu152OE2 in the structure of B*2704:β_2m:pLMP2 (2.72 Å) and B*2706:β_2m:pLMP2 (3.3 Å), (Figure 3.31 and Table 3.8).

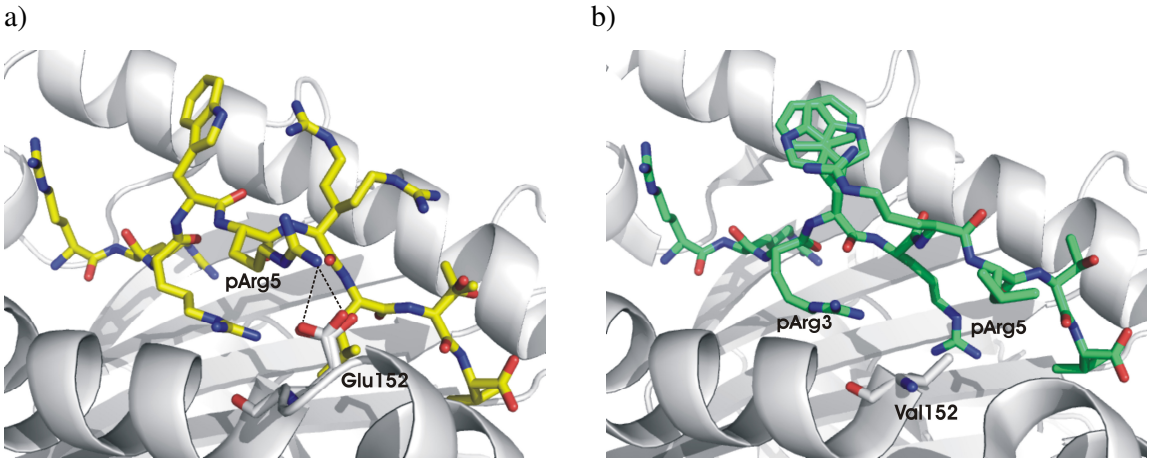

Figure 3.31. Consequences of Val to Glu change in B*2705 and B*2704/B*2706. a) novel salt bridge between polymorphic residue Glu152 and pArg5 in B*2704:β_2m:pLMP2 structure, b) the conformation of residue Val152 in B*2705:β_2m:pLMP2 structure.

Val152 (located in the middle of the α2 helix) in B*2705/09 is neutral and short and can not make contacts to any atoms of the peptide residues whereas Glu152 which occurs at this position in B*2704 and B*2706 is negatively charged and has a longer side chain which enables

contact with positively charged pArg5. Probably due to this connection pArg5 side chain is directed towards the α2 domain and not to the binding groove what might explain the conformation of the pLMP2 peptide in B*2704 and B*2706 subtypes.

The side chain of the pLeu7 residue in p4α occupies a back part of the E-pocket of the binding groove whereas in the p6α conformation this location is impossible due to pArg5 which already fill up the large E-pocket. As a consequence of the peptide binding mode, pLeu7 in B*2705 subtype points towards the α2 helix (Figure 3.27), whereas in B*2703/04/06/09 pLeu7 is inserted deeper than in B*2705.

The Asp77Ser exchange in B*2704 and B*2706 seems not to influence drastically the peptide conformation. Ser77 which resides in the α1 helix is slightly shorter than Asp and not charged resulting in a longer distance between the peptide residue and Ser77 and therefore weaker interaction. Asp77 in B*2703/05/09 interacts with the pVal9 backbone via hydrogen bond, while in case of B*2704 and B*2706, Ser77 forms additionally two hydrogen bonds to the pThr8 due to double conformation of p8 (Table 3.7 and 3.8).

The C-terminal part of the peptide is more regular than the central part of the peptide, and buried in the binding groove in all subtypes compared here, however the distal area of pLMP2 in B*2703/04/06 subtype inserts deeper than in B*2705 (Figures 3.27, 3.28, 3.29). This might be a consequence of the p4α conformation since this relationship has already been observed in B*2709 where the viral peptide is always bound in the canonical manner.

The comparison of HLA subtypes in complexes with pLMP2 indicates that sequence similarity in the binding groove does not determine the peptide binding mode. Even when the amino acid sequence in the floor of the binding groove remains identical, closely related HLA subtypes may bind the same peptide similarly, as in case of B*2703 and B*2704, or present it differently (B*2705). Surprisingly, amino acid exchanges in this region, between B*2703 or B*2704 and B*2709 or B*2706, results in almost identical peptide presentation.

3.3.2.3 Structural analysis of the pVIPR binding mode in complexes with B*2703, B*2704, B*2705, B*2706 and B*2709

So far, only the structures of B*2705:β_2m:pGR (Rückert et al., 2005) and B*2705:β_2m:pVIPR (Hülsmeyer et al., 2004) showed a dual conformation (called p4α and p6α) of the peptide. Interestingly, the pVIPR peptide in complex with B*2703 revealed exclusively the p6α conformation with negligible changes of the indole ring of pTrp4 (Figure 3.32) in comparison

with its position seen in B*2705:β_2m:pVIPR-p6α. Consequently, the binding mode of pVIPR in B*2703 is very different from the binding mode of this peptide found in B*2709 (Figure 3.32 b).

a) b)

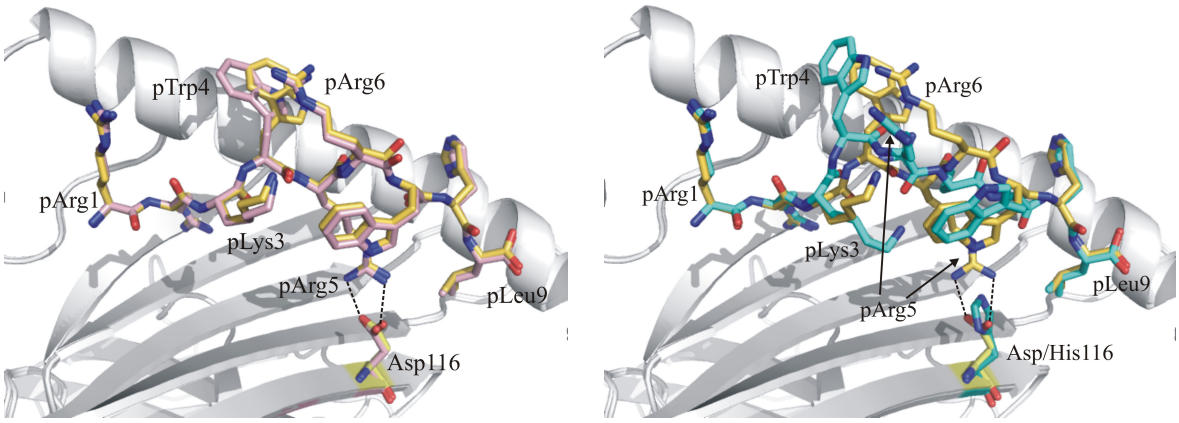

c)

TCR / α1-helix / Peptide / α2-helix / β-sheet	pArg1	pArg2	pLys3	pTrp4	pArg5	pArg6	pTrp7	pHis8	pLeu9
B*2703 (p6α)	↑	↙	↗	↖	↓	↑	↘	↖	↓
B*2705 (p6α)	↑	↙	↗	↖	↓	↑	↘	↖	↓
B*2709 (p4α)	↑	↙	↘	↑	↗	←	→	↖	↓

Figure 3.32. Structural comparison of pVIPR as presented by B*2703, B*2705 (non-canonical conformation) and B*2709. Structures overlay of: a) B*2703 (yellow) and B*2705 (pink) in complex with pVIPR –both in p6α conformation, and b) B*2703 (yellow) and B*2709 (cyan) in complex with the same peptide. The view point is from the α2-helix, which was removed for better visualization. The side chain of the polymorphic residue, Asp116 in B*2705 and in B*2703 or His116 in B*2709 is marked according to the peptide color code. The salt bridges between pArg5 and Asp116 in the B*2703:β_2m:pVIPR and B*2705:β_2m:pVIPR structures are marked with dashed lines, c) Schematic diagram showing the side chains orientations of pVIPR peptide in B*2703, B*2705 (in p6α conformation) and B*2709 binding groove. The *shaded areas* indicate structural similarity between the pVIPR peptide as presented by B*2703, B*2705, and B*2709.

In contrast, the same peptide when bound to B*2704 and B*2706 adopts the conformation extremely similar to p4α of B*2705 and B*2709. Only slight deviations of some residues can be noticed whereas the peptide backbones overlay nicely in both cases, as demonstrated in figure 3.33 and 3.34. While B*2705 presents the peptide to equal ratios in p4α and p6α conformation (50 % in p4α and 50 % in p6α), in both B*2704 and B*2706 the pVIPR peptide adopts only one conformation (Figure 3.33). It was anticipated that at least in the B*2704

subtype pVIPR might reveal also a p6α conformation like in B*2705, since the amino acid sequence in the floor of the binding groove remains conserved in both subtypes.

a)

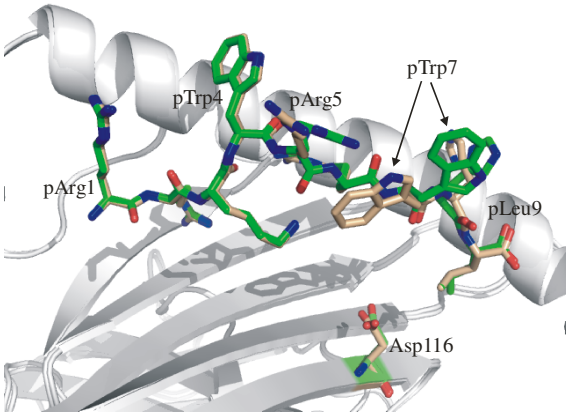

b)

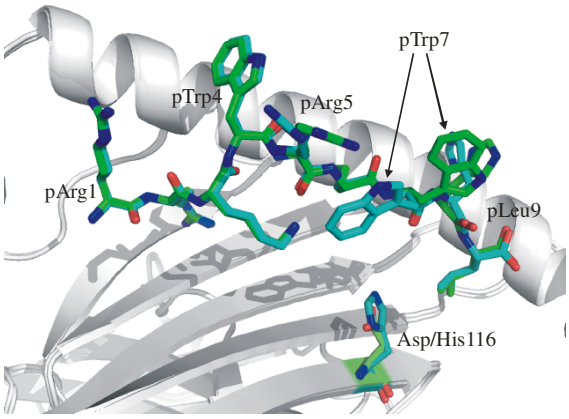

c)

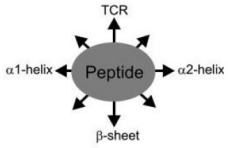		**pArg1**	**pArg2**	**pLys3**	**pTrp4**	**pArg5**	**pArg6**	**pTrp7**	**pHis8**	**pLeu9**
	B*2704 (p4α)	↑	↙	↘	↑	↗	←	↗	↖	↓
	B*2705 (p4α)	↑	↙	↘	↑	↗	←	→	↖	↓
	B*2709 (p4α)	↑	↙	↘	↑	↗	←	→	↖	↓

Figure 3.33. Structural comparison of pVIPR as presented by B*2704, B*2705 (canonical conformation) and B*2709. Comparison of crystal structures of: a) B*2704:β_2m:pVIPR (green) with B*2705:β_2m:pVIPR-p4α (light pink) and b) B*2704:β_2m:pVIPR (green) with B*2709:β_2m:pVIPR (cyan). The view point is from the α2-helix, which was removed for the better visualization. The side chain of the polymorphic residue, Asp116 in B*2705 and in B*2704 or His116 in B*2709 is marked according to the peptide color code. c) Schematic diagram showing the side chains orientations of pVIPR peptide in B*2704, B*2705 (in p4α conformation) and B*2709 binding groove. The *shaded areas* indicate structural similarity between the pVIPR peptide as presented by B*2704, B*2705, and B*2709.

a)

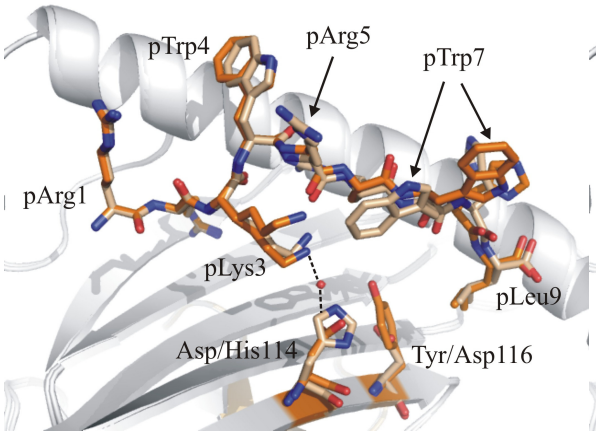

b)

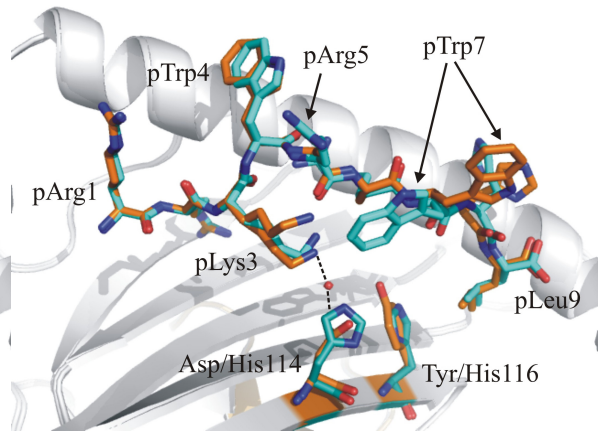

c)

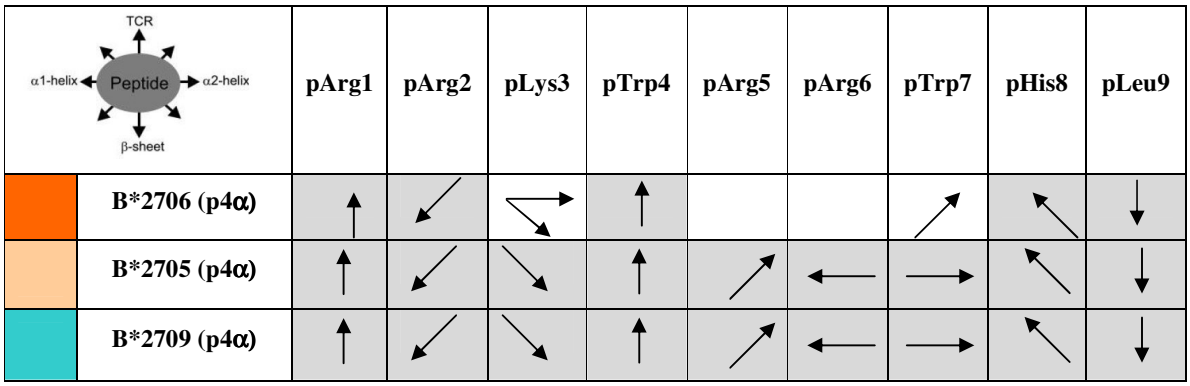

Figure 3.34. Structural comparison of pVIPR as presented by B*2706, B*2705 (canonical conformation) and B*2709. Comparison of crystal structures of: a) B*2706:β_2m:pVIPR (orange) with B*2705:β_2m:pVIPR-p4α (light pink) and b) B*2706:β_2m:pVIPR (orange) with B*2709:β_2m:pVIPR (cyan). The view point is from the α2-helix, which was removed for better visualization. The side chains of the polymorphic residues, Asp114 and Tyr116 in B*2706, His114 and Asp116 in B*2705 or His114 and His116 in B*2709, are marked according to the peptide color code. The water mediated contact between pLys3 and Asp114 in B*2706:β_2m:pVIPR structure is marked with dashed lines. c) Schematic diagram showing the side chains orientations of pVIPR peptide in B*2706, B*2705 (in p4α conformation) and B*2709 binding groove. The *shaded areas* indicate structural similarity between the pVIPR peptide as presented by B*2706, B*2705, and B*2709.

Despite the differences in peptide conformation between B*2705 and the subtypes B*2703, B*2704 and B*2706, the N terminal amino acids of pVIPR have identical position in all complexes described here. This phenomenon has already been observed for structures of these subtypes with the pLMP2 peptide.

Detailed analysis of peptide binding modes revealed also that the p3 side chain shows only negligible changes (Figure 3.32, 3.33 and 3.34) with exception of B*2706 where one of the pLys3 conformations is shifted up and the other one points towards the groove and indirectly contacts the polymorphic Asp114 (Figure 3.34 and Table 3.9). It is highly possible that this interaction prevents pArg5 to Asp114 contact and influence the overall peptide conformation.

The indole ring of pTrp4 in B*2704 has identical position as in B*2705:β_2m:pVIPR-p4α and B*2709 (Figures 3.33) and almost identical as in B*2706 (Figure 3.34) while in B*2703 p4 is shifted in the direction of C-terminus of the peptide (Figure 3.32).

While the structure of the self peptide in B*2703 is extremely similar to B*2705:β_2m:pVIPR-p6α (Figure 3.32), a drastic change is seen between structures of B*2704/B*2706:β_2m:pVIPR and B*2705:β_2m:pVIPR-p6α or B*2703:β_2m:pVIPR in the middle part of the peptide. It is possible that p4α conformation of the peptide in B*2706 is a consequence of a novel, water-mediated hydrogen bond formed between pLys3 and Asp114 (Figure 3.34). The importance of interaction between p3 and Asp114 has been already noticed in complex of B*2706 with viral peptide. Positions of p5 and p6 of pVIPR bound to B*2704 resembles the conformation of these two amino acids found in p4α binding mode of B*2705 and B*2709 with slight deviations of p5 side chain. As already mentioned it was not possible to model pArg5 and pArg6 side chains in the structure of B*2706:β_2m:pVIPR, and therefore a detailed comparison of this structure with B*2705/09:β_2m:pVIPR is not possible. However, we can surely conclude that the peptide backbone position in B*2706 differs significantly from its conformation observed in complex of B*2705:β_2m:pVIPR-p6α.

Table 3.9 Comparison of pVIPR peptide coordination in the B*2703, B*2704, B*2706 and B*2705 subtypes. Only direct intrapeptide contacts and contacts between pVIPR and HC residues are included, and solvent-mediated interactions are omitted. van der Waals' contacts are not given explicitly for each amino acid. In B*2705 A corresponds to p4α conformation B corresponds to p6α conformation.

Peptide position	B*2703:β_2m:pVIPR				B*2704:β_2m:pVIPR				B*2706:β_2m:pVIPR				B*2705:β_2m:pVIPR			
	Peptide residue	**Contact residue**	**Dist [Å]**	**Interaction**	**Peptide residue**	**Contact residue**	**Dist [Å]**	**Interaction**	**Peptide residue**	**Contact residue**	**Dist [Å]**	**Interaction**	**Peptide residue**	**Contact residue**	**Dist [Å]**	**Interaction**
pArg1 pArg2 pLys3	Contacts formed by pArg1, pArg2 and pArg3 are very similar in all complexes															
pTrp4	Solvent-exposed				Solvent-exposed				Solvent-exposed				Solvent-exposed			
	pTrp4^{O} pTrp4	pLys3^{NZ} Ile66, Ala69	2.9 ~3.3	HB vdW	No direct contact to peptide or HC residues				No direct contact to peptide or HC residues				pTrp4^{O} A pTrp4^{O} B pTrp4 B	pArg6^{NH2} pLys3^{NZ} pArg6	3.0 2.8 ~ 3.3	HB HB vdW
pArg5	Burried				Solvent-exposed				Solvent-exposed				Burried			
	pArg5^{NH1} pArg5^{NH1}	Asp116^{OD1} Asn97^{OD2}	3.0 3.1	SB HB	pArg5^{O} pArg5	Gln155^{NE2} Ile66, Gln155	3.1 3.6 -4.0	HB vdW	Side chain has not been modeled due to lack of electron density				pArg5^{NH1} B pArg5^{NH2} B	Asp116^{OD1} Asp116^{OD2}	3.04 3.10	SB SB
pArg6	Solvent-exposed				Solvent-exposed				Solvent-exposed				Solvent-exposed			
	pArg6^{NH1} pArg6	pTrp4^{O} pTrp4	3.3 ~3.3	HB vdW	pArg6	Arg69, Lys70, Gln155	3.4-4.0	vdW	Side chain has not been modeled due to lack of electron density				pArg6^{NH1} A pArg6^{NH1} A	Ile66^{O} pLys3^{O}	2.7 3.0	HB HB
pTrp7	Burried				Solvent-exposed				Solvent-exposed				Burried			
	pTrp7	Trp147, Val152 Leu156, pArg5	~3.5 -4.0	vdW	pTrp7	Glu152^{OE2}(A), Trp147	3.4	vdW	pTrp7^{N} pTrp7	Glu152^{OE2} Trp147, Ala150, Glu152	3.2 3.4-4.0	HB vdW	pTrp7^{NE1} pTrp7 A,B	Gln155^{OE1} Trp147, Val152, Leu156	3.5 ~3.5~4.0	HB vdW
pHis8	Solvent-exposed				Solvent-exposed				Solvent-exposed				Solvent-exposed			
	pHis8^{ND1}	Asp77^{OD1}	2.8	HB	pHis8^{ND1} pHis8^{O}	Glu76^{OE1} Trp147^{NE1}	2.8 3.0	HB HB	pHis8^{NE2} pHis8^{O}	Glu76^{OE2} Trp147^{NE1}	3.4 3.0	HB HB	pHis8^{ND1}	Asp77^{OD1}	2.9	HB
pLeu9	pLeu9^{N}	Asp77^{OD1}	3.0	HB	pLeu9^{N}	Ser77^{OG}	3.2	HB	pLeu9^{N}	Ser77^{OG}	2.9	HB	pLeu9^{N} pLeu9^{N}	Asp77^{OD1} Asp77^{OD2}	3.1 3.5	HB HB

Table 3.10 Comparison of pVIPR peptide coordination in the B*2703, B*2704, B*2706 and B*2709 subtypes. Only direct intrapeptide contacts and contacts between pVIPR and HC residues are included, and solvent-mediated interactions are omitted. van der Waals' contacts are not given explicitly for each amino acid.

Peptide position	B*2703:β_2m:pVIPR				B*2704:β_2m:pVIPR				B*2706:β_2m:pVIPR				B*2709:β_2m:pVIPR			
	Peptide residue	**Contact residue**	**Dist [Å]**	**Interaction**	**Peptide residue**	**Contact residue**	**Dist [Å]**	**Interaction**	**Peptide residue**	**Contact residue**	**Dist [Å]**	**Interaction**	**Peptide residue**	**Contact residue**	**Dist [Å]**	**Interaction**
pArg1 pArg2 pLys3	Contacts formed by pArg1, pArg2 and pArg3 are very similar in all complexes															
pTrp4	Solvent-exposed				Solvent-exposed				Solvent-exposed				Solvent-exposed			
	pTrp4^{O} pTrp4	pLys3^{NZ} Ile66, Ala69	2.9 ~3.3	HB vdW	No direct contact to peptide or HC residues				No direct contact to peptide or HC residues				pTrp4	Arg62, Gln65, Ile66,	~3.9	vdW
pArg5	Burried				Solvent-exposed				Solvent-exposed				Solvent-exposed			
	pArg5^{NH1} pArg5^{NH1}	Asp116^{OD1} Asn97^{OD2}	3.0 3.1	SB HB	pArg5^{O} pArg5	Gln155^{NE2} Ile66, Gln155	3.1 3.6 -4.0	HB vdW	Side chain has not been modeled due to lack of electron density				pArg5^{NH1}	Glu155^{OE1}	3.3	HB
pArg6	Solvent-exposed				Solvent-exposed				Solvent-exposed				Solvent-exposed			
	pArg6^{NH1} pArg6	pTrp4^{O} pTrp4	3.3 ~3.3	HB vdW	pArg6	Arg69, Lys70, Gln155	3.4- 4.0	vdW	Side chain has not been modeled due to lack of electron density				pArg6	Lys70, Thr73	~3.9	vdW
pTrp7	Burried				Solvent-exposed				Solvent-exposed				Burried			
	pTrp7	Trp147, Val152 Leu156, pArg5	~3.5 -4.0	vdW	pTrp7	Glu152^{OE2}(A), Trp147	3.4	vdW	pTrp7^{N} pTrp7	Glu152^{OE2} Trp147, Ala150, Glu152	3.2 3.4- 4.0	HB vdW	pTrp7^{NE1} pTrp7	Glu155^{OE1} Trp147, Val152 Leu156	3.5 ~3.5- 4.0	HB vdW
pHis8	Solvent-exposed				Solvent-exposed				Solvent-exposed				Solvent-exposed			
	pHis8^{ND1}	Asp77^{OD1}	2.8	HB	pHis8^{ND1} pHis8^{O}	Glu76^{OE1} Trp147^{NE1}	2.8 3.0	HB HB	pHis8^{NE2} pHis8^{O}	Glu76^{OE2} Trp147^{NE1}	3.4 3.0	HB HB	pHis8^{ND1}	Asp77^{OD1}	2.8	HB
pLeu9	pLeu9^{N}	Asp77^{OD1}	3.0	HB	pLeu9^{N}	Ser77^{OG}	3.2	HB	pLeu9^{N}	Ser77^{OG}	2.9	HB	pLeu9^{N} pLeu9^{N}	Asp77^{OD1} Asp77^{OD2}	3.1 3.5	HB HB

Interestingly in the structure of B*2704 and B*2706, both with pVIPR, the side chain of pTrp7 has a different position than in B*2703, B*2705 and B*2709. The pTrp7 of the self peptide in B*2704 and B*2706 is definitely pointing out of the binding groove and is more solvent exposed as it is in B*2705 or B*2709. In the subtypes B*2703/05/09 pTrp7 is directed to the α2-helix which is caused by interaction with hydrophobic Val152 (Table 3.9 and 3.10) In case of B*2704 and B*2706, the charged Glu152 pushes the hydrophobic indole of pTrp7 out of the groove what evidence an influence of polymorphic residue 152 on the side chain of peptide. The C-terminal part of pVIPR is again almost identically located in all structures which were compared in this study, however the influence of polymorphic residues in B*2704 and B*2706 localized outside the bottom of the binding groove can be also noticed. Asp77 in B*2703/05/09 interacts with the imidazole of pHis8 and the backbone of pLeu9 via hydrogen bonds, while Ser77 in B*2704 and B*2706 does not allow to fix the conformation of pHis8 and contacts only the backbone of pLeu9 (Table 3.9 and 3.10).

Although all five subtypes are closely related, they present the same peptide in two different manners and it is difficult to explain the binding mode of pVIPR in B*2703, B*2704 and B*2706. Despite the sequence identity in the floor of the binding groove in B*2703, B*2704 and B*2705, the peptide is presented by B*2704 differently than in B*2703 and B*2705. It is surprising that an exchange of two amino acids at the bottom of the groove between B*2704/B*2709 and B*2706 results in p4α conformation of pVIPR in all three subtypes.

3.4 Production of HLA-B27:β_2m:pEBV8TvE-KIR3DL1 complexes

3.4.1 Construct of a KIR3DL1 clone for expression in *E.coli*

The clone containing vector pASK-IBA6 which encoded the extracellular part of KIR3DL1 was already available in the Institut für Immungenetik. The vector was obtained from IBA GmbH, Göttingen and contains the Strep-Tag II and Factor Xa at its N-terminus. Additionally Flag-Tags and a His-Tag were added to the sequence to improve the purification step in case the affinity chromatography would be used. The schematic representation of the construct for transformation is shown on figure 3.35. *E. coli* cells were transformed as described in Materials and Methods. The DNA was isolated from a single colony and was sequenced to check it for the absence of mutations.

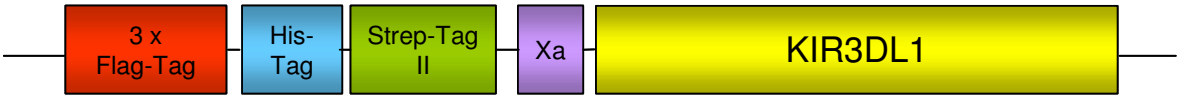

Figure 3.35. Schematic representation of KIR3DL1 construct for the expression in bacteria. Factor Xa (violet) and the StrepTag II (green) were already included in the original sequence of vector pASK-IBA6. Additionally the Flag-Tags (red) and His-Tag (blue) were added. The yellow part represents KIR3DL1 sequence of the extracellular part.

3.4.2 KIR3DL1 protein expression in *E. coli*

Three different expression strains of *E.coli,* Origami (DE3), BL21 (DE3) and TG1, were transformed with the construct (Figure 3.35) in order to check the protein production yield. BL21 (DE3) expressed the KIR3DL1 protein in the largest amount, about 15 mg/300 ml of bacterial culture.

The extracellular part of KIR3DL1 was expressed in *E.coli* in the form of inclusion bodies according to the protocol which is described in details in section 2.2.7.1. Small deviations from the protocol were introduced in order to obtain better expression yield. The cells with vector were growing well at 37°C; however, lower temperature yielded better protein expression. Therefore after induction the culturing temperature was changed to 30°C and the time of expression was extended to O/N incubation. The concentration of the inclusion body proteins in urea buffer was calculated on the basis of extinction coefficient factor which was obtained from the ProtParam program of ExPasy (www.expasy.org).

To check the quality of the produced inclusion bodies, KIR3DL1-InB was loaded on SDS gels using reducing conditions. Figure 3.36 illustrates that the purity of the protein inclusion bodies which were produced is very good. From one liter of bacteria culture we were able to obtain protein in appropriate amounts, about 40-50 mg (see 2.2.7.1)

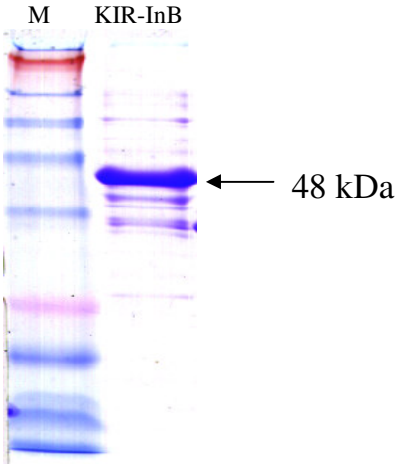

Figure 3.36. Analysis of inclusion body quality on SDS gel stained with Coomassie Blue. M is See Blue Plus2, molecular weight marker. The band with a size about 48 kDa corresponds to the KIR3DL1 inclusion body protein.

3.4.3 Refolding of KIR3DL1

KIR3DL1 was thus successfully expressed as inclusion body protein in *E. coli;* however inclusion bodies are thought to contain misfolded protein. Therefore, unfolding with urea and refolding of the protein was necessary to proceed with KIR3DL1 in a functional form. Both the KIR3DL1 molecule and in complex with HLA-B27 was produced in the hope to aid refolding. In the following section various conditions and their results of KIR3DL1 reconstitution are shown. In these experiments size exclusion chromatography was performed using a Superdex 200 column which was calibrated previously with BSA (67 kDa), Ovalbumin (43 kDa), Chymotrypsin A (25 kDa), Cytochrome C (12.5 kDa) and Aprotinin (6.5 kDa). This allowed estimating according to the size of mentioned proteins in which fractions the complex or KIR3DL1 molecule would be obtained.

3.4.3.1 Refolding of the KIR3DL1 molecule

Different conditions of refolding buffer were tested with diverse amounts of protein added and resulted in highly aggregated protein. Numerous deviations from the protocol (Materials and Methods, section 2.2.7.2) were implemented in order to minimize the amount of aggregate. The method using higher pH (8.5), 1 mM glutathione-oxydized, 20 % glycerol, and glutathione-reduced added 24 hrs after setting up the refolding was described for proteins which contain cysteines by Rudolph and Lilie, 1996. Trehalose dihydrate (Singer and Lindquist, 1998) and carbohydrate polymers NV molecules called Stabil-PAC NV10 (Novexin) were suggested to help in decreasing protein aggregation. All tested conditions of reconstituting KIR molecule are summarized in table 3.11. None of them afforded KIR3DL1 as a monomer, as checked by size exclusion chromatography and SDS-PAGE.

Table 3.11. Conditions of reconstitution of KIR3DL1 and results. Standard reconstitution buffer refers to the buffer described in Materials and Methods (section 2.1.2) with pH 7.5. Any deviations from this are mentioned in the table. All reconstitutions were carried out at 4°C.

Nr	mg of KIR3DL1 per 100 ml of refolding buffer	Type of buffer	Time of reconstitution	Result
1.	2 mg	standard, pH 7.5	2 weeks	KIR in aggregate
2.	4 mg	standard, pH 7.5	2 weeks	KIR in aggregate
3.	4 mg	standard, pH 7.5	5 days	KIR in aggregate
4.	2 mg	standard, pH 8.5	2 weeks	KIR in aggregate
5.	4 mg	pH 8.5, 1 mM glutathione-oxyd., 20 % glycerol, glutathione-red. added after 24 hrs	1week	KIR in aggregate
6.	4 mg	pH 8.5, 1 mM glutathione-oxyd., 20 % glycerol, glutathione-red. added after 24 hrs	2 weeks	KIR in aggregate
7.	4 mg	pH 7.5, 1 mM glutathione-oxyd., glutathione-red. added after 24 hrs, 10 % trehalose	1 week	KIR in aggregate
8.	4 mg	pH 7.5, 1 mM glutathione-oxyd., glutathione-red. added after 24 hrs, 10 % trehalose	2 weeks	KIR in aggregate
9.	4 mg	pH 7.5, 1 x STABIL-PAC NV10	1 week	KIR in aggregate

A typical example of the purification result is shown on the FPLC chromatogram and on the SDS gel in figure 3.37. In case of this trial 4 mg of KIR3DL1 were refolded for 2 weeks in a standard reconstitution buffer and conditions.

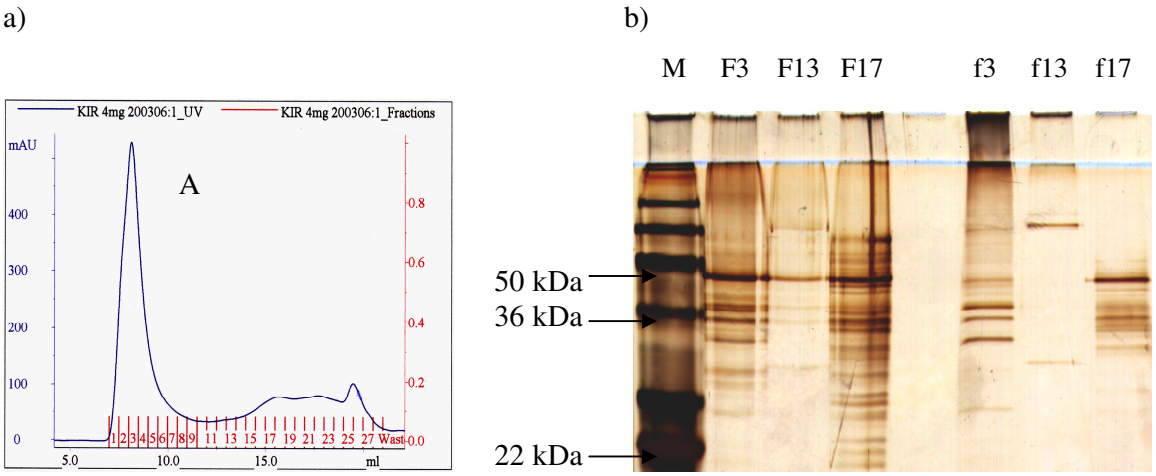

Figure 3.37. Chromatogram of size exclusion purification of KIR3DL1 reconstitution and SDS gel analysis. a) Chromatogram showing results of KIR refolding and purification. According to the size the KIR3DL1 protein should be in fraction 17. The peak obtained in fractions 2-6 (A) corresponds to aggregated protein. b) Silver staining of 13 % SDS-PAGE run under non-reducing and reducing conditions. F3, F13 and F17 correspond to number of fraction from chromatogram run under reducing conditions, f3, f13 and f17 refer to fraction number run under non-reducing conditions. M is See Blue Plus2, molecular weight marker.

Purification of the protein resulted in a large amount of aggregated material (fractions 2-6) whereas KIR3DL1 in monomeric state was obtained in only very small amounts (fraction 17) and with moderate purity which is seen on figure 3.37 (b). In the aggregate fractions as well as in fraction 17 (corresponding with size to monomeric KIR3DL1), protein was detectable, however the amount of it was much higher in the aggregate peak.

Since we were not able to obtain suitable amounts of monomeric KIR3DL1 alone due to intensive aggregation of the molecule, the fractions containing aggregates were collected and treated with 10 M Urea and 2 mM DTT and the mixture was applied to refolding buffer containing 20 % glycerol. However, after two weeks of reconstitution no improvement of KIR refolding could be observed.

3.4.3.2 Reconstitution of HLA-B27:β_2m:pEBV8TvE-KIR3DL1 complexes

Production of KIR3DL1 in complex with one of the B27 subtypes could stabilize the protein and allow to continue with crystal production. Among all subtypes which were so far investigated in the Institut für Immungenetik B*2705 forms one of the best complexes. Therefore we used B*2705 for experiments with KIR3DL1 at first. However, B*2704 and B*2706 were also tested for complex formation with KIR3DL1. The extracellular domains of B*2705, B*2704 and B*2706 as well as β_2m were expressed in *E. coli* as described in Materials and Methods. The peptide which was used (pEBV8TvE) is known to protect the cell from NK cell lysis and should thus permit binding of KIR3DL1. In the next section the refolding trials of KIR3DL1 with HLA-B27 subtypes are described.

3.4.3.2.1 Complex formation of B*2704 and B*2706 with KIR3DL1

The inclusion body proteins (B*2704 or B*2706) in soluble form were set up for refolding with peptide pEBV8TvE (RRIYDLITL) and KIR3DL1. Several reconstitution conditions were tested to find the best ones for complex formation. In table 3.12 the reconstitution conditions and results are given.

Table 3.12. Conditions of KIR3DL1 reconstitution in complex with B*2704 and B*2706 and obtained results. Standard reconstitution buffer refers to the buffer described in Materials and Methods (section 2.1.2) with pH 7.5. The amount of peptide was each time the same and equal 1 mg per 100 ml of buffer. Any deviations from it are mentioned in the table. All reconstitutions were incubated at 4°C.

Nr	Molar ratio of components in refolding buffer	Type of buffer	Time of reconstitution	Result
1.	B*2704:β_2m:KIR 1 : 2.5 : 1	standard, pH 7.5	2 weeks	KIR in aggregate
2.	B*2706:β_2m:KIR 1 : 2.5 : 1.5	standard, pH 7.5	2 weeks	KIR in aggregate
3.	B*2706:β_2m:KIR 1 : 2.5 : 1	pH 7.5, 20 % glycerol, 2 mM glutathione-red.	2 weeks	KIR in aggregate
4.	B*2704:β_2m:KIR 1 : 2.5 : 1 (KIR added one week later)	pH 7.5, 20 % glycerol, 2 mM glutathione-red.	2 weeks	KIR in aggregate

Double amounts of reduced glutathione as well as 20 % glycerol were formerly tested for protein stabilization; therefore these conditions were used in experiments to minimize the amount of aggregated protein. However, none of tested conditions improved complex formation. The figure below shows an exemplary size exclusion chromatography profile and SDS-PAGE analysis of KIR3DL1 with B*2704 refolding experiment.

a) b)

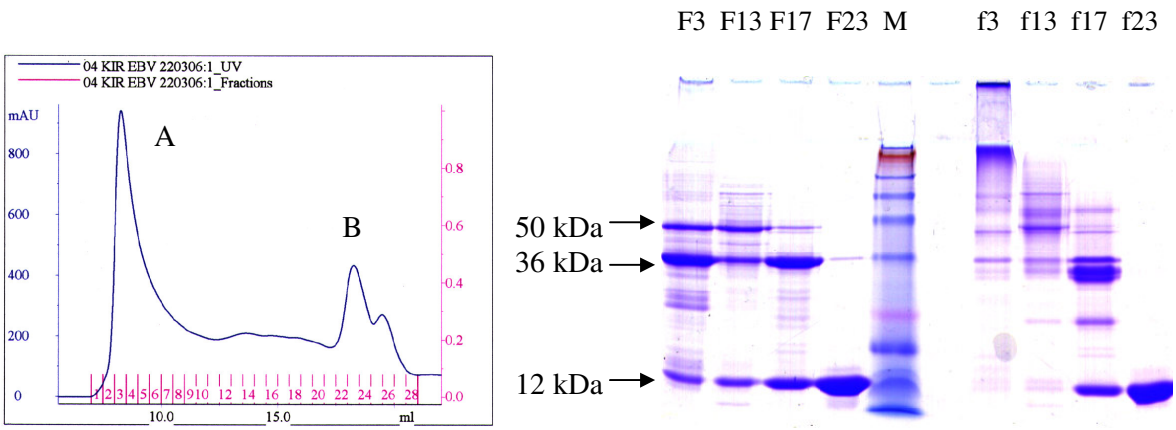

Figure 3.38. Chromatogram of size exclusion purification of KIR with B*2704 reconstitution and SDS gel analysis. a) Chromatogram showing results of B*2704:β_2m:pEBV8TvE-KIR3DL1 purification. According to the size the protein complex of B*2704:β_2m:pEBV8TvE-KIR3DL1 should be in fraction 13. The peak (A) obtained in fractions 2-6 corresponds to aggregates of protein, peak B (fractions 22-24) refers to free β_2m. b) Coomasie staining of SDS gel run under non-reducing and reducing conditions. F3, F13, F17 and F23 correspond to number of fraction from chromatogram run under reducing conditions, f3, f13, f17 and f23 refer to fraction number run under non-reducing conditions. M is See Blue Plus2, molecular weight marker. The band of about 48 kDa size corresponds to KIR3DL1, the one of 36 kDa size to HC and the band of 12 kDa size to β_2m.

Similarly as in case of KIR alone, it was not possible to obtain pure complex of KIR with B*2704 or B*2706 due to intensive aggregation of KIR. The amount of tetramer which was produced (about 0.17 mg/ml) was not suitable for crystallization and not pure enough. Therefore, the fractions containing aggregates were collected and treated with 10 M Urea and 2 mM DTT. The mixture was applied to the refolding buffer containing 20 % glycerol and double amount of reduced glutathione. However, no improvement in HLA-B27-KIR complex formation could be observed after two weeks of reconstitution.

3.4.3.2.2 Complex formation of B*2705 with KIR3DL1

Experiments with B*2705 were mainly done with the peptide pEBV8TvE (RRIYDLITL), which is an immunodominant viral peptide EBV, modified at position p8 (Stewart-Jones et al., 2005). It was reported that HLA-B*2705:β_2m:pEBV complex does not allow KIR3DL1 binding but this property is restored when E at p8 is changed to T.

The inclusion body proteins (B*2705, β_2m and KIR3DL1) in soluble form were set up for refolding with peptide. Several reconstitution conditions were tested to establish the ones which allow for the best complex formation. Table 3.13 illustrates all trials which were performed in order to produce a B*2705:β_2m:pEBV8TvE-KIR complex.

Table 3.13. Conditions of KIR reconstitution in complex with B*2705 and obtained results. Standard reconstitution buffer refers to the buffer described in Materials and Methods (section 2.1.2) with pH 7.5. The amount of peptide was each time the same, 1 mg per 100 ml of buffer. Any deviations from the protocol are mentioned in the table. All reconstitutions were incubated at 4°C. Conditions which gave best result are marked with green.

Nr	Molar ratio of component per 100 ml of refolding buffer	Type of buffer	Time of reconstitution	Result
1.	B*2705:β_2m:KIR 1 : 2.5 : 1	standard, pH 7.5	2 weeks	KIR in aggregate
2.	B*2705:β_2m:KIR 1 : 2.5 : 1.5	standard, pH 7.5	2 weeks	KIR in aggregate
3.	B*2705:β_2m:KIR 1 : 2.5 : 1 (KIR added one week later)	pH 7.5, 10 % glycerol	2 weeks	KIR in aggregate (0.35 mg/ml) and in complex with B*2705:β_2m:pep (0.2 mg/ml)
4.	purified complex (B*2705:β_2m) + KIR 1 : 2.5 : 1	pH 7.5, 10 % glycerol	1 week	KIR in aggregate

5.	purified complex (B*2705:β_2m) + KIR 1 : 2.5 : 1	pH 7.5, 10 % glycerol	2 weeks	KIR in aggregate
6.	B*2705:β_2m:KIR 1 : 2.5 : 2	pH 7.5, 10 % glycerol	2 weeks	KIR in aggregate (1.4 mg/ml) and in complex with B*2705:β_2m:pep (0.25 mg/ml)
7.	B*2705:β_2m:KIR 1 : 2.5 : 2	pH 7.5, 20 % glycerol, 2 mM glutathione-red.	2 weeks	KIR in aggregate (0.7 mg/ml) and in complex with B*2705:β_2m:pep (0.2 mg/ml)
8.	B*2705:β_2m:KIR 1 : 2.5 : 1	pH 8.5, 1 mM glutathione-oxyd., 20 % glycerol, glutathione-red. added after 24 hrs	2 weeks	KIR in aggregate (0.8 mg/ml) and in complex with B*2705:β_2m:pep (0.25 mg/ml)
9.	KIR 24h hrs later added B*2705 and β_2m 1 : 2.5 : 1	pH 8.5, 1 mM glutathione-oxyd., 20 % glycerol, glutathione-red. added after 24 hrs	1 week	KIR mostly in aggregate
10.	B*2705:β_2m:KIR + KIR – InB in Guanidinium HCl 1 : 2.5 : 1 : 1	pH 8.5, 1 mM glutathione-oxyd., 20 % glycerol, glutathione-red. added after 24 hrs	2 weeks	KIR in aggregate
11.	KIR – InB in Guanidinium HCl 24h hrs later added B*2705:β_2m 1 : 2.5 : 1	pH 8.5, 1 mM glutathione-oxyd., 20 % glycerol, glutathione-red. added after 24 hrs	2 weeks	KIR in aggregate
12.	B*2705:β_2m:KIR 1 : 2.5 : 1	pH 7.5, 10 mM 4-mercaptophenylacetic acid	1 week	KIR in aggregate
13.	B*2705:β_2m:KIR 1 : 2.5 : 1	pH 7.5, 10 mM 4-mercaptophenylacetic acid	2 weeks	KIR in aggregate
14.	B*2705:β_2m:KIR 1 : 2.5 : 1 (KIR added one week later)	pH 7.5, 10 mM 4-mercaptophenylacetic acid	1 week	KIR in aggregate

The standard reconstitution conditions for KIR3DL1 complex formation with HLA-B27 subtypes were done according to Garboczi et al. (1992), and were employed formerly in the Institut für Immungenetik for the formation of HLA-B27 complexes. All deviations from this protocol were performed in order to decrease the amount of aggregate which was always obtained in the majority for KIR3DL1 and HLA-B27 reconstitution trials. The influence of higher pH (8.5), 1 mM glutathione-oxyd, 20 % glycerol, and reduced glutathione added after 24 hrs after setting up the refolding was previously studied (Rudolph and Lilie, 1996), and was advised for proteins which contain cysteines. Therefore these conditions have been tested in experiments with KIR3DL1 reconstitution with the B*2705 subtype. Also

4-mercaptophenylacetic acid was suggested to help in reconstitution of cysteine-rich proteins (Gough et al., 2006). Variations in molar ratio of components and time of refolding were also tested to produce complexes of high purity and in appropriate quantities.

Similar to the situation with complexes of KIR with B*2704 and B*2706 as well as KIR alone, intensive aggregation of the molecules was observed when reconstituted with B*2705. The fractions containing aggregates were combined and treated with 10 M urea and 2 mM DTT in order to separate the aggregates. The mixture was applied to refolding buffer containing 20 % glycerol and double amount of reduced glutathione. After two weeks of reconstitution the aggregate fell slightly apart and allowed HLA-B*2705-KIR complex formation. However, the amount of protein was insufficient for further experiments.

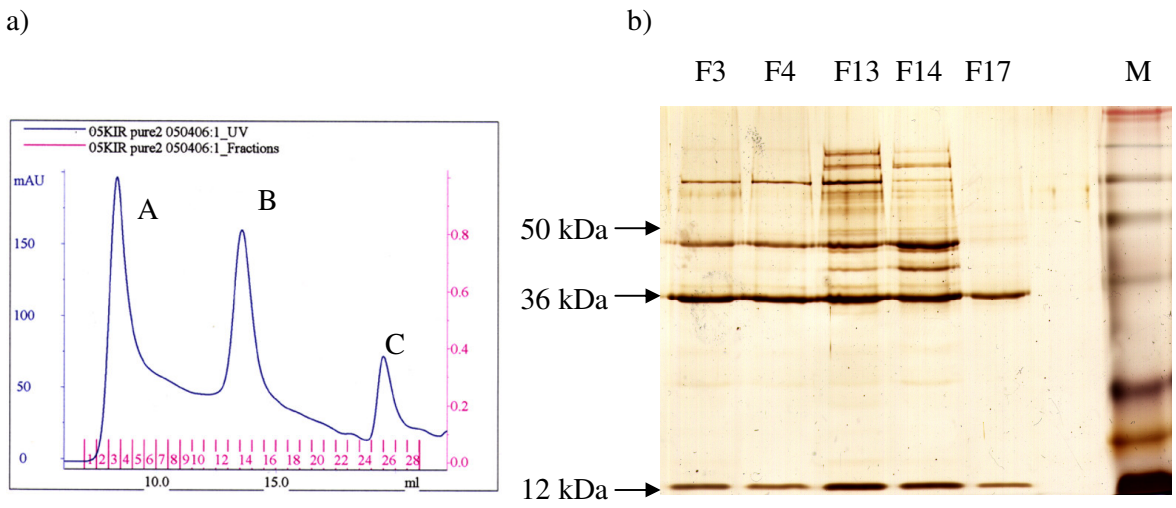

Figure 3.39. Purification efficiency of the re-refolding experiment for the B*2705-KIR aggregate-containing fractions and its analysis on the SDS gel. a) The chromatogram shows the results of size exclusion purification of a second refolding of aggregate-containing fractions of B*2705:β_2m:pEBV8TvE-KIR reconstitution. The Superdex 200 column was used to purify the complex. According to the size peak A corresponds to aggregates, peak B contains KIR3DL1 in complex with B*2705:β_2m:pEBV8TvE, and peak C free β_2m. b) Silver staining of 13 % SDS-PAGE run under reducing conditions. F3, F4, F13, F14 and F17 correspond to number of fraction from chromatogram. M is See Blue Plus2, molecular weight marker.

The chromatogram in Figure 3.39 shows that the aggregate-containing peak A (fractions 2-5) is slightly higher than the complex-containing peak B (fractions 13-14). SDS-PAGE analysis confirmed that fractions 13 and 14 contain components of B*2705:β_2m:pEBV8TvE-KIR complex, however, their purity was insufficient.

The pEBV8TvE peptide prevents from NK cell lysis and is known to enhance the binding of the inhibitory receptor KIR3DL1 to the pMHC. In this study two other peptides with ability to provide protection from NK-mediated lysis were used, pNK (RRIKAIIHK) and MV-F (RRYPDAVYL) as well as two which do not preclude NK cell lysis: npNK (RRIKAITLK) and np1NK (RRYQKSTEL). All peptides were tested for the ability to form complexes with pMHC

and KIR. Refolding conditions were based on the previously established ones and gave the best complexes, when KIR was added about one week later in comparison to the pMHC complex. Surprisingly, complexes of all four peptides after purification by size exclusion chromatography gave the peaks in fractions where the complex of B*2705:β_2m:peptide with KIR3DL1 was expected. This was in line with expectations for pNK and MV-F but not for the two other peptides (npNK and np1NK) which should not allow binding of KIR3DL1 to B*2705:β_2m:peptide. This indicates that the reconstitutions did not provide the desired result.

Finally, the refolding of B*2705 and KIR in the absence of peptide was tested. Standard amounts of B*2705 (3 mg), β_2m (2.5 mg) and KIR (4 mg) were applied to 100 ml of reconstitution buffer and incubated at 4°C for 5 days. As in case of pMHC, KIR protein was mostly obtained as aggregate and a small amount in complex with B*2705. This result could indicate that the peptide presentation in the binding groove is not needed for HLA-KIR interaction under the *in vitro* conditions, clearly a contradiction to the *in vivo* results.

In another attempt to produce B*2705:β_2m:pEBV8TvE in complex with KIR3DL1, an additional molecule was used in order to stabilize the KIR3DL1 in complex with HLA-B27 subtype. The leukocyte immunoglobulin-like receptor-1 (LIR1) molecule is known to interact also with HLA-B27 molecules (Chapman et al., 2000; Allen et al., 2001; Willcox et al., 2003) and was added to the reconstitution mixture. LIR is a membrane glycoprotein expressed only on a subset of NK cells, on monocytes, dendritic, B and T cells (Borges et al., 1997; Colonna et al., 1997; Cosman et al., 1997; Colonna et al., 1998). The extracellular part of the protein has about 25 kDa size and contains two immunoglobulin-like domains, which are related to KIR domains. The molecule binds to the α3 helix of HLA and to β_2m (Chapman et al., 1999; Willcox et al., 2003; Shiroishi et al., 2003). It was expected that LIR might play a role as stabilizer of pMHC-KIR3DL1 complexes and that this would help to avoid aggregation of complexes. The BL21 cells containing LIR1 cloned to pET23a(+) vector were already available in the Institut für Immungenetik, and used for inclusion body preparation. In this experiment we used LIR in unfolded form as well as refolded and purified LIR by size exclusion. Both proteins were very pure and of good quality.

Both unfolded and pure refolded proteins were set up for a standard reconstitution and for reconstitution with modifications, where KIR was added one week later, and LIR was added two days after KIR, or LIR was mixed together with B*2705, β_2m and peptide and KIR was added 2 days later. In all cases, half the amount of LIR in comparison to KIR (molar ratio) was used in order to prevent high amounts of LIR-B27 complex formation. After purification by size exclusion chromatography the characteristic pattern of chromatogram for

B*2705:β_2m:pEBV8TvE-KIR3DL1 was always obtained with an additional peak. Based on column calibration and size of the peak it was supposed that this is the LIR molecule. However, the fractions corresponding to the size of B*2705:β_2m:pEBV8TvE-KIR complex formed again a very slight peak in comparison with the large amount of aggregate. To verify which components are contained in each peak fractions four fractions were analyzed on SDS gel under reducing and non-reducing conditions. The result of the experiment is shown in figure 3.40.

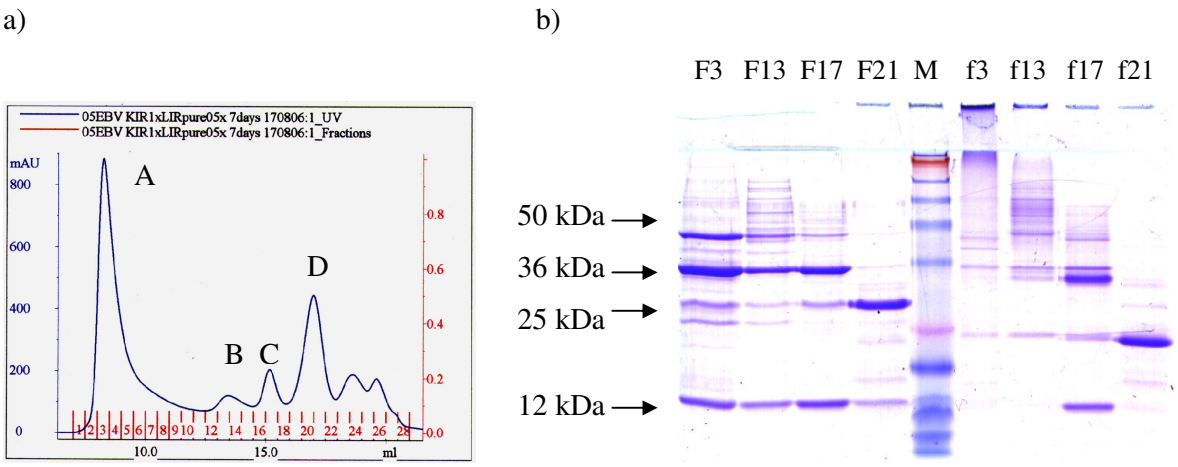

Figure 3.40. Purification results of B*2705-LIR-KIR reconstitution and analysis of size exclusion chromatography fractions in an SDS gel. a) Chromatogram of size exclusion purification of B*2705-KIR complex (peak B). Peak A corresponds to aggregates of components, peak C to ternary complex B*2705:β_2m:pEBV8TvE, peak D possibly contains LIR. b) Coomasie staining of 13 % SDS gel with non-reducing and reducing conditions testing fractions of the FPLC run. F3, F13, F17 and F21 correspond to fraction number run under reducing conditions, whereas f3, f13, f17 and f21 correspond to fractions run under non-reducing conditions. M is See Blue Plus2, molecular weight marker.

The chromatogram (Figure 3.40 a) shows purification results of B*2705-KIR production in presence of LIR. Using these reconstitution conditions it was possible to produce complex of B*2705:β_2m:pEBV8TvE-KIR3DL1 (peak B), however, the largest part of KIR occurs again as aggregate (peak A). Some B*2705 does not bind KIR and is present in fraction 17 in complex with light chain and peptide. According to its size, the LIR molecule is present in fraction 21 (peak D). On the gel all components of the reconstitution mixture can be seen. Fraction 3 contains aggregates of complexes, fraction 13 corresponds to heterotetramer (B*2705:β_2m:pEBV8TvE-KIR3DL1) and contains all three molecules, the upper band (about 48 kDa) representing KIR, middle band – heavy chain (32 kDa) and lower band – light chain (12 kDa).

All tested conditions for refolding of KIR3DL1 in complex with HLA-B27 (different reconstitution conditions, various peptides tested, reconstitution of KIR alone as well as in complexes with B*2705 and additionally with LIR1) resulted mostly in the aggregation of the

components. The best complex formation was observed when KIR was added about one week later than the other components of the reconstitution (Table 3.13, marked with green color). These conditions for complex formation were also tested in shorter time intervals. The time was reduced between B*2705:β_2m:pEBV8TvE and KIR adding to refolding buffer (to 3 days) as well as the time of reconstitution of all components (to 5 days). There was no significant change in complex formation after shortening of time. The FPLC chromatogram and SDS gel analysis of KIR3DL1 reconstitution with B*2705:β_2m:EBV8TvE are presented in figure 3.41.

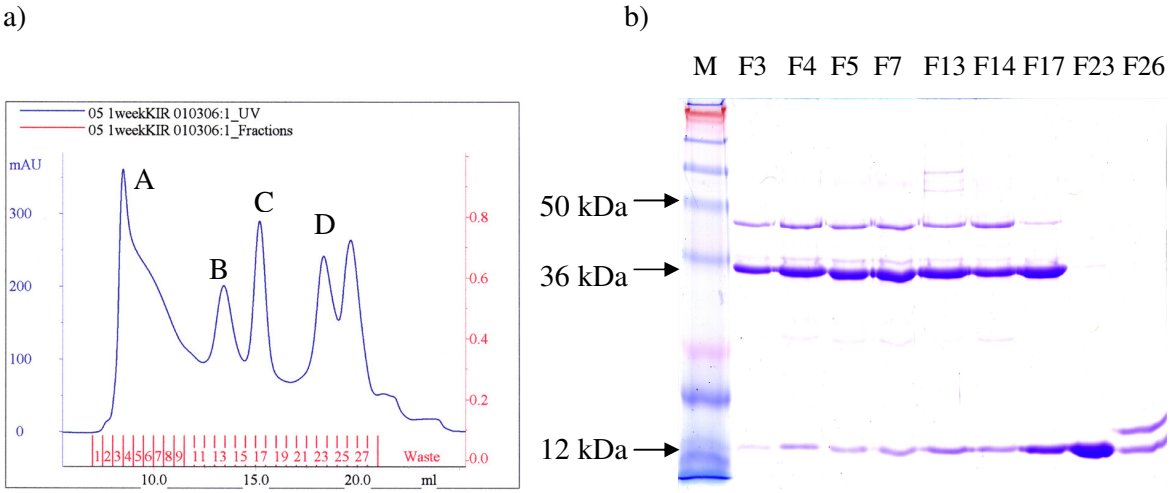

Figure 3.41. Chromatogram of size exclusion purification of KIR with B*2705 subtype reconstitution and its analysis on 13 % SDS gel. a) Chromatogram showing results of B*2705:β_2m:EBV8TvE-KIR purification. According to the size peak A corresponds to aggregates of the components, peak B to quaternary complex of KIR3DL1with B*2705:β_2m:pEBV8TvE, peak C to ternary complex of B*2705:β_2m:pEBV8TvE, peak D possibly contains free β_2m. b) Comassie Blue staining of SDS gel run in reducing conditions. F3, F4, F7, F13, F14, F17, F23 and F26 correspond to number of fraction from chromatogram. M is See Blue Plus2, molecular weight marker.

The B*2705:β_2m:EBV8TvE-KIR3DL1 complex was obtained in fraction 13 (peak B). The peak A obtained in fractions 2-6 corresponds to aggregates of protein, Fraction 17 (peak C) refers to the HLA complex with the peptide and fraction 23 (peak D) to free β_2m. Figure above (3.41, panel b) proves that fraction 13 contains all components of the B*2705:β_2m:EBV8TvE-KIR3DL1 complex. The most upper band (about 48 kDa) represents KIR3DL1, the lower band, about 36 kDa, the heavy chain of HLA, and the band at the bottom (12 kDa) corresponds to β_2m (also shown in fraction 23 as a separate band).

Comparison of the stoichiometrical ratios between fractions loaded on SDS-PAGE gel shows that in fractions F4, F5, F7, F13 and F14 all complex components are present, whereas in F3 and F17 proportion of components is disrupted. Bands corresponding to the light chain and KIR3DL1 in F3 and F17 respectively are very thin, possibly pointing to the little amount of KIR molecule not bound to the HLA complex in case of F17. The size of the molecule which was

obtained in fraction F13 and particularly F14 is consistent with the HLA-B27-KIR complex and it contains best proportions of its elements, whereas in F4, F5 and F7 higher amounts of heavy chain and lower amounts of light chain can be seen (Figure 3.40 b). Since after one week of reconstitution, the aggregation of components was unchanged in comparison to the two-weeks refolding, a time curve of refolding was performed. KIR3DL1 was added one week after the B*2705, β_2m and pEBV8TvE peptide, and the mixture was checked for complex formation after 4 hrs, 1 day, 2 days and 3 days. Already after 4 hrs of reconstitution of KIR3DL1 with B*2705:β_2m:pEBV8TvE, high aggregation was noticed (results not shown).

To check whether the protein that was produced for complex formation is KIR3DL1, a mass spectrum was taken using MALDI-TOF/TOF method. For this purpose the purified complex of B*2705:β_2m:pEBV8TvE-KIR was separated on a 13 % SDS gel (not shown) and the bands which corresponded in size to KIR3DL1 in aggregate fraction and in fraction containing complex of HLA molecule with KIR were cut out and applied to MALDI-TOF/TOF, to prove protein identity. This experiment was performed by the Mass Spectrometry Group (Dr. E. Krause) at the Leibniz-Institut für Molekulare Pharmakologie in Berlin-Buch. MALDI-TOF/TOF analysis confirmed that in the complex of B*2705:β_2m:pEBV8TvE-KIR as well as in the aggregate the KIR3DL1 is present and has the expected molecular mass.

Using the above mentioned conditions, where KIR was added one week later and has been reconstituted with B*2705:β_2m:pEBV8TvE for one week, complexes were prepared for crystallization. Since the amount of pure protein which could be produced was still not suitable for conventional crystallization screens, the B*2705:β_2m:pEBV8TvE-KIR3DL1 complexes were setup for crystallization in the Protein Structure Factory (PSF). The new techniques which are employed here allow to set up crystallization experiments using very small amounts of material (0.1 µl drop containing protein). Purified complex of B*2705:β_2m:pEBV8TvE-KIR3DL1 was concentrated to 7 -12 mg/ml and used for preparing crystallization set-up.

3.4.4 Crystallization trials of KIR in complex with B*2705:β_2m:pEBV8TvE

Various conditions of protein crystallization were employed in order to obtain crystals of KIR3DL1 in complex with B*2705:β_2m:pEBV8TvE. Yvette Roskie from Protein Structure Factory (PSF) performed the following screens: SaltHT screen, Hampton screen, HuMag screen, IndexHT screen and PEG Ion screen. A wide spectrum of conditions was tested, i.e. various salts at different concentrations and pH as well as different concentrations of salts in combination

with PEG, glycerol, 2-propanol, imidazole. All of them were performed at 20°C and at 4°C. The only microcrystal was obtained from 25% PEG 4000 0.2M $(NH_4)_2SO_4$ in Hamptonscreen C10 performed at 20°C, from 20% PEG 6000, 0.1M Citric acid pH 5.0 made at 4°C and from 10% PEG 3000, 0.2M $ZnCH_3CO_2$ 0.1M $NaCH_3CO_2$ pH 4.6 performed at 4°C. However, the size and the quality of the crystal did not allow harvesting and X-ray data collection. Also attempts of reproducing the crystal were unsuccessful.